

1 **Response to Anonymous Referee #1 re: Report #1 on Revised Manuscript**

2  
3 We are very thankful for the referee's continued assistance in improving our manuscript. We believe that  
4 an acceptable conclusion has been reached regarding the issue of air-surface exchange. Our comments are  
5 found embedded in the referee's text below in red.

6  
7 **Report #1**

8 **Submitted on 18 Nov 2013**

9 **Anonymous Referee #1**

10  
11 Summary: The authors have addressed some of the points raised, but not all of them. The model may be  
12 suitable to simulate exposure near the sources, but not in remote areas, which cover certainly more than  
13 half of the domain, at least not for semivolatiles, due to insufficient process resolution (air-surface  
14 exchange).

15 I recommend to reject the paper or insist that the results are limited to non-volatile PAHs (as suggested in  
16 the review to the submitted version).

17 Description of model used:

18 Sufficient in the revised version

19  
20 Gas-particle partitioning – discussion of unplausible model results:

21 The authors refuse to discuss, but plan to address in a subsequent publication.

22  
23  
24 Air-surface exchange and model evaluation by comparison with observed data / choice of monitoring sites:  
25 The authors maintain that the neglect of air-surface exchange is insignificant as these "parametrizations  
26 likely have a minor effect in regions subject to ongoing PAH emissions" and "atmospheric PAH burdens in  
27 North America are likely not dominated by air-surface exchange".

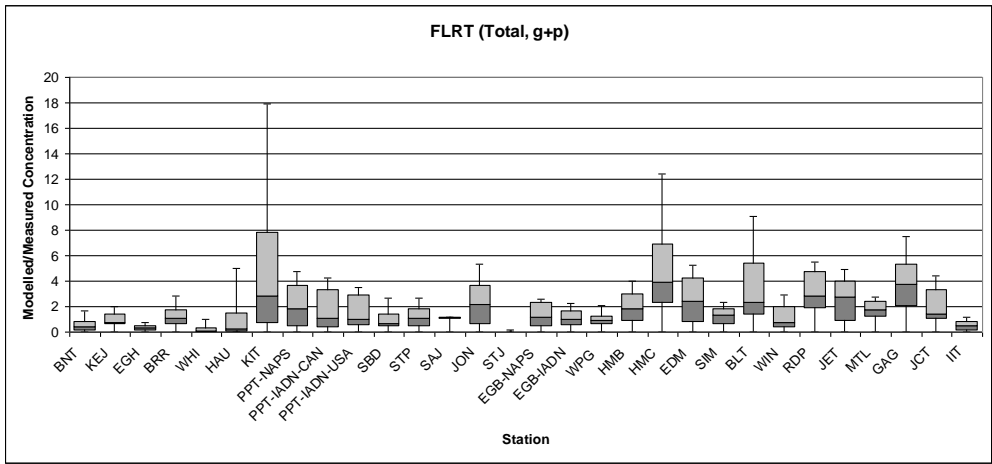
28 However, in model study with air-surface exchange considered it was found for two semivolatile PAHs  
29 addressed in the Galarneau et al. study (anthracene and fluoranthene) that volatilization from soil exceeds  
30 depositions in summer not only in remote areas of North America (the US West, British Columbia,  
31 Ontario), but also in areas certainly influenced by sources (the US Midwest, southern Ontario, California)  
32 (Fig. S7b in Lammel et al., 2009). The reason is that the characteristic travel distance from the source in  
33 combination with lifetimes in soil lead to burdens in soil, decreasing with distance from source, which turn  
34 into secondary emissions and may seasonally exceed the deposition of advected primary and secondary  
35 emissions and model will underpredict concentrations at remote sites.

36  
37 The atmospheric levels of fluoranthene and pyrene, respectively, are expected to drop to 37% and 14% (1/e  
38 and 1/e<sup>2</sup>, respectively) within characteristic travel distances from the sources of 160-450 km and 320-900  
39 km, respectively. (These ranges conservatively represent upper estimates as based on the climatological 24-  
40 hour mean oxidant level, (0.38-1.24)x10<sup>6</sup> OH cm<sup>-3</sup> within the model domain (Spivakovsky et al., J.  
41 Geophys. Res. 2000), while more PAH is emitted during day-time.)

42  
43 **As also noted by a third referee, the potential impact of air-surface exchange needs to be acknowledged**  
44 **more fully in our manuscript and we have conducted the following analyses to support our new revision.**

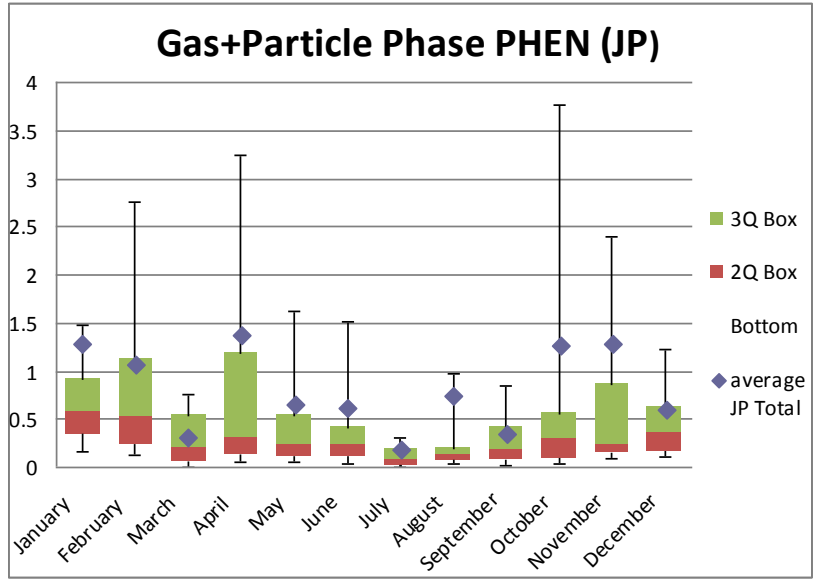
45  
46 **We have re-plotted the site-specific FLRT results with the x-axis now depicting measurement sites in**  
47 **increasing order of population within 25km. As can be seen in the figure, there is no clear relationship**  
48 **between population and underestimation by the model. In fact, the highest population of 3.86 million at IIT**  
49 **(Chicago) exhibits one of the lowest overall modelled-to-measured ratios.**

50



51  
52  
53  
54  
55  
56  
57  
58  
59

However, as a result of referee comments, we have also replotted our data by month as shown below for PHEN. As can be seen in the figure, the model underprediction is greatest in summer which is consistent with the absence of volatilisation (or other potential missing sources or overestimated sinks). We observe a similar pattern for the other volatile PAHs (ANTH, FLRT and PYR) but not for the less volatile BaA, C+T and BaP. Since such behaviour is consistent with volatilisation in summer months, we have acknowledged this limitation on the volatile PAH results in our abstract and have included new figures and discussion (3.1.1) in the latest revision of the manuscript.



60  
61  
62  
63  
64  
65  
66

The authors insist that the spatial resolution (42km) is high enough to reproduce the gradients in urban areas. "As seen in Figure 4, the model performance does not differ much between sites." However, the sites indicating worst model performance (modelled/measured <0.1), WHI and STJ, are remote sites, unlike most other sites tested.

67 We apologize for the miscommunication. We did not mean to suggest that 42km resolution reproduces  
68 gradients in urban areas, but rather that this regional resolution is able to reproduce a substantial portion of  
69 the gradient between urban and rural areas.  
70  
71

72 **Response to Anonymous Referee #3 re: Report #2 on Revised Manuscript**

73  
74 We are very thankful to the third referee for taking the time to review our revised manuscript. Responses  
75 to the report are embedded below in red.

76  
77 **Report #2**

78 **Submitted on 08 Dec 2013**

79 **Anonymous Referee #3**

80  
81 The authors need to re-write the latter part of Section 3.1.1 (Results & Discussion) and include a new figure  
82 (see referee report)

83  
84 The authors present a revised manuscript detailing a modelling study that simulates PAH air  
85 concentrations across North America using a Eulerian CTM model. The simulation is based on  
86 the year 2002 and includes 7 PAHs that cover a relatively wide range in physical-chemical  
87 properties. This is one of only a handful of studies that has attempted to predict air concentrations  
88 at high spatial-resolution for these chemicals and considerable effort has been expended on gas-  
89 particle partitioning given the semi-volatile nature of these compounds.

90 The primary emissions of PAHs appear to be very well handled and detailed. These build on a  
91 methodology previously published by the lead author. Similarly a thorough model description is  
92 provided on the various fate/behaviour processes, including the use of two gas/particle  
93 partitioning approaches. The results are usefully presented including a thorough comparison with  
94 measurement data (modelled/measured ratios). I believe the paper is of publishable quality for  
95 ACP. However, the authors need to do more to address the concerns raised by a previous  
96 reviewer regarding the contribution of temperature-driven re-emission from secondary sources.  
97 Below are two

98 key points which the authors need to highlight/address:

99 (1) For the 7 PAHs studied here secondary sources (re: air-surface exchange) are most pertinent  
100 for phenanthrene (PHEN). Its isomer anthracene (ANTH) is probably too reactive for this  
101 processes to be fully significant (i.e. its half-life in air and soil is relatively short, plus its presence  
102 in air is erratic and can be driven in the main by notable point/primary sources).

103  
104 The emissions inventory developed by the lead author was based on an extensive collection of  
105 published emissions data. No difference in emissions sources between PHEN and ANTH was  
106 observed; all sources had emissions of both isomers though the proportions varied among  
107 sources.

108  
109 The relative importance of losses through OH reactivity will likely have an important effect on the  
110 total mass of the different volatile PAHs. Both emissions from air-surface exchange and losses  
111 due to OH reactivity would likely be at a maximum in the summer. Hence, while ANTH's  
112 increased OH reactivity might make it disappear from the air more quickly than PHEN, one might  
113 still observe patterns consistent with air-surface exchange. PAH emitting activities with a strong  
114 seasonal cycle (e.g. biomass burning) may also contribute to some of the missing summer mass.  
115 A test of the sensitivity of model results to the relative magnitudes of these processes would be  
116 interesting to pursue.

117  
118 For the higher MW 4-ringed PAHs of fluoranthene and pyrene the magnitude of temperature—  
119 driven re-emission from secondary sources will be low relative to primary emissions (particularly  
120 over a single summer season re: 2002). Secondary emissions are negligible for the high MW  
121 PAHs (e.g. B[a]P). The authors need to make these points clear in the manuscript and cite  
122 studies that have observed this phenomenon and provide a few quantitative details (i.e. the  
123 observed seasonality in low MW PAH concentrations brought about by secondary reemission)  
124 (there are plenty of good studies in the literature for soil, water bodies, vegetation and urban  
125 surfaces).

126

127 Please see our analysis below for information regarding the 4- and 5-ring species. We have  
128 added statements to Section 3.1.1 regarding the existing literature.  
129

130 (2) Section 3.1.1. para (line 419-434). The authors discuss the model results with regards to the  
131 exclusion of air-surface exchange in their model. This paragraph is essential but I disagree with  
132 the flow of their discussion as they state that the model summary results provide indefinite  
133 evidence. Far from it(!) – the model appears to be working very well - and from the evidence  
134 provided both in Table 1 (summary comparison between model and measured) and Fig 3, the  
135 model appears to fit with PAH behaviour as described in point (1) above. For PHEN, the model  
136 clearly under predicts the air concentrations. There is nothing ambiguous about this and the  
137 underestimated PHEN concentrations in the model must presumably be due to the reemission  
138 component which is missing from the model. This is fine and not a problem for the manuscript,  
139 but the authors need to state this clearly and examine this issue more carefully and include this  
140 observation/finding in the abstract. For example, I would like to see a map of the spatial  
141 distribution of model/measurement ratios for PHEN, for both winter (i.e. Dec – Feb) and summer  
142 (i.e. June-Aug). The hypothesis here is that the ratios will be closer to 1 in the winter and deviate  
143 further from 1 in the summer (i.e. as the re-emission component becomes more relevant during  
144 the warmer part of the year). The authors should 'play up' this part of the paper and not try to  
145 discount discrepancies as ambiguous or uncertain. Another case in point is ANTH. As  
146 ANTH is relatively volatile it is not surprising that the model average is below the  
147 measurement average (again akin to PHEN re: re-emission component) but the data are variable  
148 and skewed (hence similar model/measured medians). This is just what I would expect for ANTH  
149 released from notable point sources but with a relatively short half-life. In short, the authors need  
150 to highlight the role played by air-surface exchange on PHEN and ANTH concentrations, and use  
151 the model results to demonstrate/quantify this process rather than discount it as model ambiguity.  
152 In fact, I believe this could be a real strength to this paper, more so than the gas-particle (g-p)  
153 partitioning story (especially as the two g-p  
154 approaches show little difference).  
155

156 Thank you for your suggestions regarding our model's systematic underprediction of  
157 phenanthrene. Such underestimation might be caused by

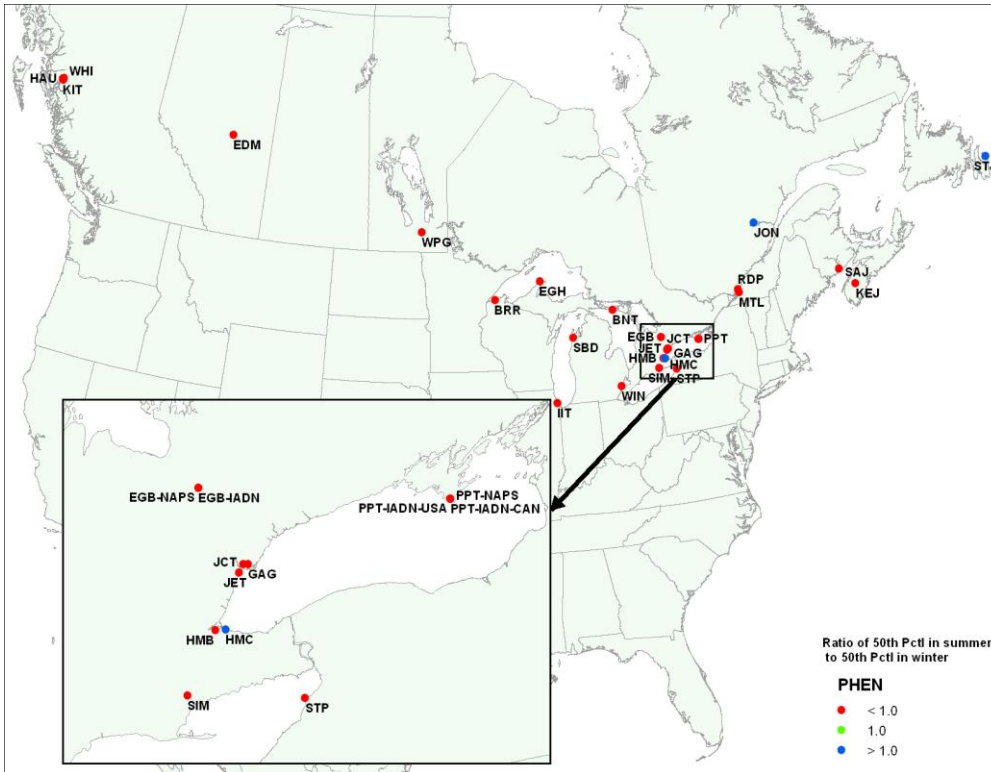
- 158 (1) underestimated emissions
- 159 (2) overestimated removal processes (OH reaction, deposition)
- 160 (3) overestimated dispersion from source areas

161 Processes within each of these three categories can be identified by examining differences or  
162 similarities between species and over spatiotemporal scales.  
163

164 If case (1) is at play and emissions are underestimated due to missing air-surface exchange, we  
165 should observe modelled-to-measured concentration ratios that

- 166 (1) vary from lower in summer to higher in winter
- 167 (2) vary from lower in rural/background locations to higher in urban/industrial locations
- 168 (3) show a systematic decrease in underprediction from the most volatile species to the least  
169

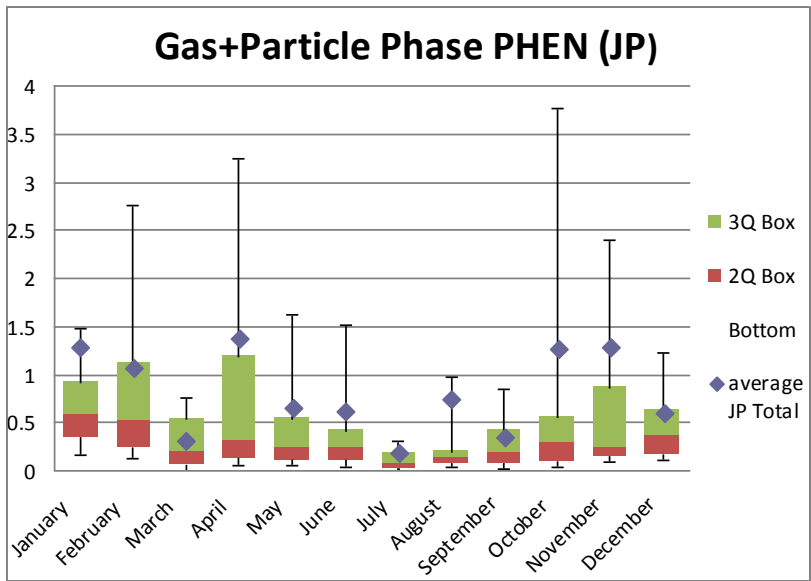
170 Attached is the figure requested by the reviewer. The modelled-to-measured concentration ratios  
171 were calculated for each site in summer and winter. The summer-to-winter ratio of the median  
172 values is plotted for each location at which measurement data were available. Modelled-to-  
173 measured concentration ratios for PHEN are indeed smaller in summer than in winter at all sites  
174 except Hamilton (Confederation Park), Jonquière, and St. John's. The first two of the latter  
175 locations are cities with substantial point source emissions from steel and aluminum processing,  
176 respectively.  
177



178  
 179  
 180  
 181  
 182  
 183  
 184  
 185  
 186  
 187  
 188

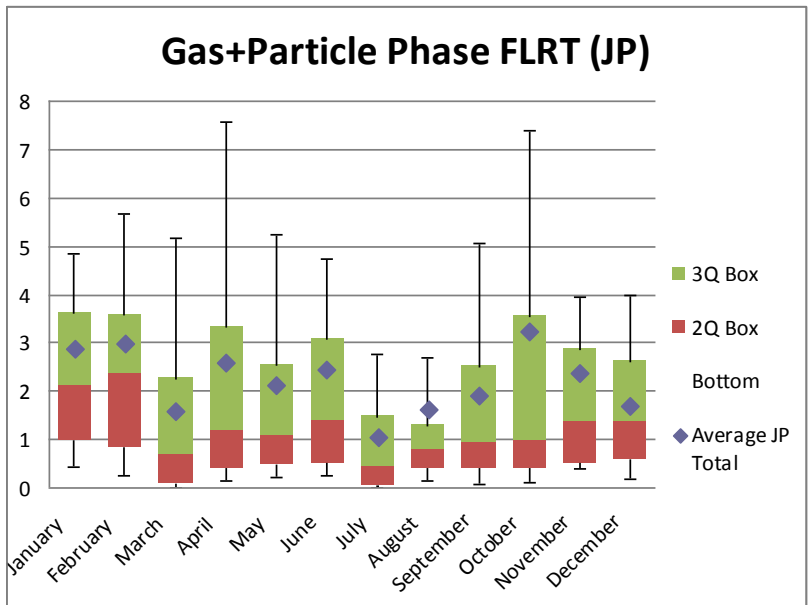
This result appears to support the argument that the underprediction of PHEN by our model is due to the missing air-surface exchange process. However, we observe similar patterns for ANTH, FLRT and PYR and not for BaA, C+T or BaP (not shown).

Since we find the map somewhat difficult to read, we have produced box-and-whisker plots of modelled-to-measured concentrations that are segregated by month. Therein we see a temporal pattern that shows greater underprediction in summer than in winter for PHEN.



189  
190  
191  
192  
193  
194  
195

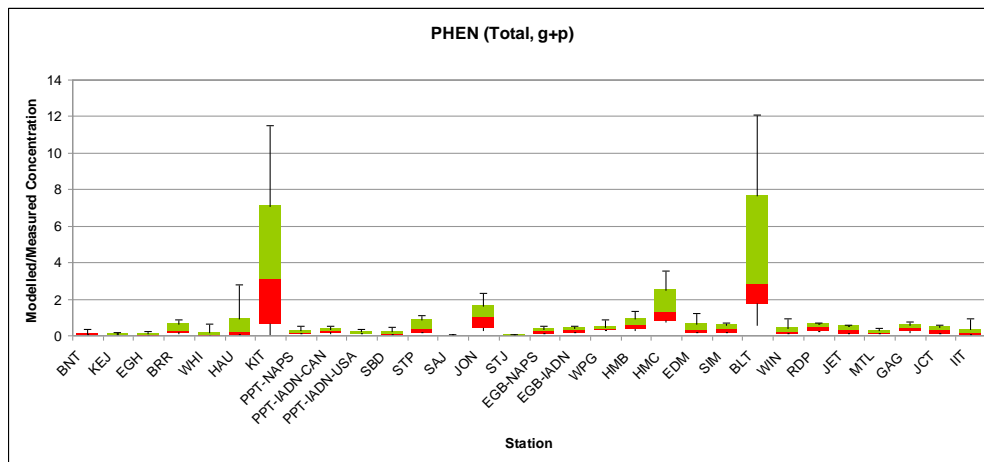
As with the maps, we see this again for the next three PAHs (increasing GC retention order/decreasing volatility). For example, FLRT exhibits a minimum in modelled-to-measured concentration ratio during the summer months. Yet this was the PAH species for which the model performed best and the referee did not expect air-surface exchange to be significant.



196  
197  
198  
199  
200

We have examined the issue in another way as well. We have plotted the box-and-whisker plots by location with the x-axis order indicating increasing population within 25km of the measurement site. If missing air-surface exchange is the cause of PHEN underprediction by the model, one

201 would expect to see the greatest underpredictions at the least populated sites and a steady  
202 increase toward equiprediction at the most populated or industrial locations.  
203



204  
205  
206 Though the figure shows overpredictions at industrial sites (e.g., Jonquière JON and Hamilton  
207 HMC) and some of the most extreme underpredictions at the most rural sites (BNT, KEJ, and  
208 EGH), the pattern is not consistent. Underpredictions are also seen at SAJ and STJ and the site  
209 with the highest population (IIT Chicago) exhibits the 10<sup>th</sup> most extreme underprediction.  
210

211 As a result of these augmented analyses, we respectfully suggest that the variation in model  
212 performance over the annual cycle is consistent with the absence of air-surface exchange.  
213 However, since ANTH, FLRT and PYR show similar temporal patterns to PHEN but are not  
214 similarly underpredicted, an additional factor must be contributing to the underprediction of  
215 PHEN. We suspect that the emissions for this species are erroneously low and we will be  
216 revisiting the inventory for future projects.  
217

218 We hope that the addition of a new two-part figure (monthly PHEN and PYR box-and-whisker  
219 plots) and the following text to Section 3.1.1 will satisfy the request made by the referee. We  
220 have also added a statement to the Abstract.  
221

222 “Though results are equivocal on an annual basis, monthly patterns observed in the model output are  
223 consistent with the absence of a seasonal source (e.g., air-surface exchange). Volatilisation from a variety  
224 of environmental compartments is typically stronger in warmer periods than in cooler ones (e.g., Nelson et  
225 al., 1998; Smith et al., 2001; Motelay-Massei et al., 2005; Bozlaker et al., 2008; Wang et al., 2011). Figure  
226 4 shows the monthly distribution of modelled-to-measured concentration ratios for PHEN and PYR. Both  
227 exhibit higher values in winter than in summer as do ANTH and FLRT whereas this seasonality is not  
228 observed for the higher molecular BaA, C+T or BaP (not shown). These findings are consistent with a  
229 missing volatilisation source that emits during warmer weather. However, other factors could also be  
230 involved including overestimated loss terms (e.g., oxidation, deposition) or underestimated emissions (e.g.,  
231 forest fires) during warmer periods. The investigation of the relevant causes is a priority for future model  
232 development. Regardless of the causes, the seasonal effect on model output appears to be compounded by  
233 further, as yet unidentified factors whereby PHEN is underpredicted throughout the year and ANTH, FLRT  
234 and PYR are overpredicted through some seasons, potentially due to air-surface exchange that leads to net  
235 deposition during cooler months.”  
236  
237  
238



239  
240  
241  
242  
243  
244  
245  
246  
247  
248  
249  
250  
251  
252  
253  
254  
255  
256  
257  
258  
259  
260  
261  
262  
263  
264  
265  
266  
267  
268  
269  
270  
271  
272

**PAH Concentrations Simulated with the AURAMS-PAH Chemical Transport  
Model over Canada and the USA**

**E. Galarneau<sup>1,\*</sup>, P.A. Makar<sup>1</sup>, Q. Zheng<sup>1</sup>, J. Narayan<sup>1</sup>, J. Zhang<sup>1</sup>, M.D. Moran<sup>1</sup>,  
M.A. Bari<sup>1,2</sup>, S. Pathela<sup>1,3</sup>, A. Chen<sup>1,3</sup>, and R. Chlumsky<sup>1,4</sup>**

<sup>1</sup> **Air Quality Research Division, Environment Canada, 4905 Dufferin Street,  
Toronto, ON, M3H 5T4, Canada**

<sup>2</sup> **Department of Public Health Sciences, School of Public Health, University of  
Alberta, Edmonton, AB, T6G 2G7**

<sup>3</sup> **Department of Computer Science, University of Waterloo, 200 University Avenue,  
Waterloo, ON, N2L 3G1, Canada**

<sup>4</sup> **Department of Environmental Engineering, University of Waterloo, 200 University  
Avenue, Waterloo, ON, N2L 3G1, Canada**

**\* Corresponding Author: Elisabeth Galarneau, [elisabeth.galarneau@ec.gc.ca](mailto:elisabeth.galarneau@ec.gc.ca)**

**Revised Manuscript**

**Submitted to  
Atmospheric Chemistry and Physics**

**[11 February 28 October 2014](#)**

## Abstract

The off-line Eulerian AURAMS (A Unified Regional Air quality Modelling System) chemical transport model was adapted to simulate airborne concentrations of seven PAHs: phenanthrene, anthracene, fluoranthene, pyrene, benz[a]anthracene, chrysene+triphenylene, and benzo[a]pyrene. The model was then run for the year 2002 with hourly output on a grid covering southern Canada and the continental USA with 42-km horizontal grid spacing. Model predictions were compared to ~5,000 24-hour-average PAH measurements from 45 sites, most of which were located in urban or industrial areas. Eight of the measurement sites also provided data on particle/gas partitioning which had been modelled using two alternative schemes. This is the first known regional modelling study for PAHs over a North American domain and the first modelling study at any scale to compare alternative particle/gas partitioning schemes against paired field measurements. The goal of the study was to provide output concentration maps of use to assessing human inhalation exposure to PAHs in ambient air. Annual average modelled total (gas + particle) concentrations were statistically indistinguishable from measured values for fluoranthene, pyrene and benz[a]anthracene whereas the model underestimated concentrations of phenanthrene, anthracene and chrysene+triphenylene. Significance for benzo[a]pyrene performance was close to the statistical threshold and depended on the particle/gas partitioning scheme employed. On a day-to-day basis, the model simulated total PAH concentrations to the correct order of magnitude the majority of the time. [The model showed seasonal differences in prediction quality for volatile species which suggests that a missing emission source such as air-surface exchange should be included in future versions.](#) Model performance differed substantially between measurement locations and the limited available evidence suggests that the model spatial resolution was too coarse to capture the distribution of concentrations in densely populated areas. A more detailed analysis of the factors influencing modelled particle/gas partitioning is warranted based on the findings in this study.

304 **1. Introduction**

305  
306 Polycyclic aromatic hydrocarbons (PAHs) are ubiquitous air pollutants that tend to be  
307 most concentrated in areas of dense human population (Hafner et al., 2005) but are also  
308 detected at locations remote from local sources (Hung et al., 2005). Many PAH species  
309 have been classified as carcinogens (IARC, 2010) and they are implicated routinely as  
310 toxicants in airborne particulate matter (Kelly and Fussell, 2012). They are regulated  
311 under international agreements such as the Aarhus Protocol on Persistent Organic  
312 Pollutants. Benzo[a]pyrene, a commonly-reported PAH species, is subject to ambient air  
313 guidelines in many jurisdictions.

314  
315 In Canada, PAHs meet the criteria for inclusion on the Toxic Substances List of the  
316 Canadian Environmental Protection Act (Environment Canada and Health Canada,  
317 1994), and the resulting government obligation has been to reduce or minimise their  
318 release into the environment. Nationwide anthropogenic emissions of benzo[a]pyrene, a  
319 commonly-reported species, fell by 70% between 1990 and 2010 according to estimates  
320 made by the National Pollutant Release Inventory (Environment Canada, 2012). Though  
321 there are no federal guidelines for PAHs in Canadian air, a recent analysis of ambient  
322 monitoring data found that measured PAH concentrations regularly exceed the health-  
323 based guidelines set by the Canadian province of Ontario (Galarneau and Dann, 2011).

324  
325 In the USA, PAHs are listed as Clean Air Act Hazardous Air Pollutants as part of the  
326 polycyclic organic matter (POM) class of compounds (US EPA, 2012) and have been  
327 identified as a regional cancer concern in the US National-Scale Air Toxics Assessment  
328 (US EPA, 2012). Industrial releases to air reported to the US Toxics Release Inventory  
329 (TRI) fell by 35% between 1995 and 2010 (US EPA, 2012). There is no federal US  
330 guideline for PAHs in ambient air.

331  
332 PAH measurements are labour-intensive compared to those of criteria air contaminants  
333 such as ozone and particulate matter, and the processes governing their atmospheric fate  
334 are not yet well-understood. In an attempt to elucidate the spatiotemporal distributions of  
335 PAH sources and ambient concentrations, several numerical modelling studies have been  
336 published. Lagrangian frameworks have been used for Europe (Van Jaarsveld et al.,  
337 1997; Halsall et al., 2001) and China (Liu et al., 2007; Lang et al., 2007; Lang et al.,  
338 2008). Others studies have used box modelling (Prevedouros et al., 2004) and  
339 multimedia fate approaches (Yaffe et al., 2001; Prevedouros et al., 2008). Eulerian  
340 chemical transport models (CTMs) have been developed for Europe (Shatalov, 2005;  
341 Aulinger et al., 2007; Matthias et al., 2009; Gusev et al., 2011; Bieser et al., 2012) and  
342 east Asia (Zhang et al., 2009; 2011a; 2011b; Inomata et al., 2012), and three such studies  
343 on a global scale have also been published in recent years ( Sehili and Lammel, 2007;  
344 Lammel et al., 2009; Friedman and Selin, 2012).

345  
346 The aforementioned studies differ in many respects relating to the PAH species  
347 examined, the temporal variability of their emissions, and the spatial resolutions and  
348 process representations in the models. None has focussed exclusively on North America  
349 at the regional scale. As well, although several particle/gas partitioning mechanisms have  
350 been explored in other models, including Junge-Pankow adsorption (Junge, 1977;

351 Pankow, 1987), organic matter sorption (Finizio et al., 1997), and combined  
352 adsorption/absorption (Dachs and Eisenreich, 2000), no previous studies have evaluated  
353 model output against paired phase-distributed measurements for alternative partitioning  
354 expressions on the same domain.

355  
356 This study presents the results of a chemical transport model, AURAMS-PAH, run over  
357 North America at 42-km horizontal grid spacing with hourly output for the year 2002.  
358 Seven PAH species were simulated with the model. Three isomer pairs of decreasing  
359 volatility and increasing particulate fraction comprise six of the species: phenanthrene  
360 (PHEN) and anthracene (ANTH) ( $178 \text{ g mol}^{-1}$ ), fluoranthene (FLRT) and pyrene (PYR)  
361 ( $202 \text{ g mol}^{-1}$ ), and benz[a]anthracene (BaA) and chrysene/triphenylene (C+T) ( $228 \text{ g mol}^{-1}$ ).  
362 The seventh PAH, benzo[a]pyrene (BaP) ( $252 \text{ g mol}^{-1}$ ), is not generally considered to  
363 be semivolatile but has been included due to its common use as a representative PAH  
364 species. Two particle/gas partitioning schemes, Junge-Pankow (JP: Junge, 1977;  
365 Pankow, 1987) and Dachs-Eisenreich (DE: Dachs and Eisenreich, 2000), were tested.

366  
367 Model performance was evaluated against ~5,000 measurements from 45 stations in  
368 established networks in Canada and the USA. This is the first published model to be run  
369 and evaluated for PAH concentrations and their distributions between the particle and gas  
370 phases using two partitioning methods. It is also the first such model to be evaluated  
371 over a regional North American domain.

372

## 373 2. Methods

374

### 375 2.1 Model Description

376

377 AURAMS (A Unified Regional Air quality Modelling System) is an Eulerian CTM  
378 originally developed to simulate criteria air contaminants. The standard version of the  
379 model uses a sectional approach to represent the size distribution of airborne particles: 12  
380 size bins from 0.01 to 40.96  $\mu\text{m}$  in diameter and 9 particulate species (sulphate, nitrate,  
381 ammonium, elemental carbon, primary organic aerosol, secondary organic aerosol,  
382 crustal material, sea salt, and aerosol water) are usually considered. The model includes  
383 process representation for tropospheric gas-phase oxidative chemistry, the absorptive  
384 formation of secondary organic aerosols, inorganic heterogeneous chemistry, particle  
385 microphysics (nucleation, condensation, coagulation, etc.), cloud processing of aerosols,  
386 advective transport, vertical diffusion, and gas and particle emissions and deposition. A  
387 detailed overall description of AURAMS appears in Gong et al. (2006) while a  
388 description of the aerosol sectional approach and the microphysics modules of the model  
389 can be found in Gong et al. (2003a,b). Performance evaluation and model  
390 intercomparison results for AURAMS appear in McKeen et al. (2008), Smyth et al.  
391 (2009), Makar et al. (2010), Kelly et al. (2012) and Solazzo et al. (2012) among other  
392 publications.

393

394 A modified version of the AURAMS CTM known as AURAMS-PAH was developed to  
395 incorporate primary semivolatile organic compounds that are subject to sorptive  
396 partitioning. Starting from the standard AURAMS CTM had the advantage that a

397 number of required fields for modelling PAHs were already available. These included  
398 hydroxyl concentration, total particle surface area, and fractions of particle elemental  
399 carbon and organic carbon. The modifications made to AURAMS version 1.3.2 in order  
400 to simulate PAHs are described below. Physico-chemical property values used for each  
401 PAH in the modified code are found in Table S1.1 of the Supplementary Material.

402  
403 *2.1.1 Dry Deposition of Gases.* Within AURAMS, gaseous dry deposition velocities are  
404 modelled using the inverse resistance analogy for several land-use categories (Zhang et  
405 al., 2002). Three resistances are assessed in AURAMS and only the first of these  
406 (aerodynamic resistance) is independent of the chemical species under consideration.  
407 The species-dependent resistances are the quasi-laminar sub-layer resistance and the  
408 surface or canopy resistance. The latter both depend on the gas-phase diffusivity of the  
409 compound in question, and this quantity was calculated in the model according to the  
410 Fuller et al. method described in Reid et al. (1987).

411  
412 Surface or canopy resistance is the most complex of the three gaseous dry deposition  
413 component resistances and tends to dominate total dry deposition (Zhang et al., 2002).  
414 One of its sub-components, mesophyll resistance, was set to  $100 \text{ s m}^{-1}$  for species that are  
415 relatively insoluble in water and have small oxidizing capacities, as is the case for PAHs.  
416 The remaining sub-components (cuticle and ground resistances) are determined by  
417 scaling to  $\text{O}_3$  and  $\text{SO}_2$  settings based on physico-chemical qualifications. For the PAHs,  
418 scaling factors to  $\text{O}_3$  and  $\text{SO}_2$  for both acetaldehyde and  $\text{C}_3$  carbonyls, the least soluble  
419 organic compounds considered in AURAMS aside from the PAHs, were used.  
420 Unsubstituted compounds such as PAHs are generally considered to have high  
421 resistances to deposition whereas carbonyl resistances are thought to be lower (Zhang et  
422 al., 2002). However, published observations of PAH deposition led us to assume that  
423 deposition velocities would be greater than zero (low resistances) and we therefore used  
424 the best-available homologues in AURAMS to represent PAHs. This is an uncertainty in  
425 the model that merits future attention.

426  
427 Volatilisation of gaseous PAHs can occur from exposed water (Hoff et al., 1996), soil  
428 (Jones, 1994), and impervious urban surfaces (Diamond et al., 2000). Net gaseous  
429 deposition to the Great Lakes in 2002 was downward (Blanchard et al., 2005) suggesting  
430 that PAH fugacities in air exceeded those in surface compartments at the regional scale.  
431 Volatilisation was not included in this first-generation version of AURAMS-PAH and the  
432 effect of this omission is presented in Section 3.1.1.

433  
434 *2.1.2 Gas-Phase Reactions.* Reactions of gas-phase PAHs with hydroxyl radicals are  
435 considered in this model. Since these reactions consume relatively little hydroxyl due to  
436 the trace concentrations of PAH, their reactions were simulated outside the AURAMS  
437 gas-phase chemistry solver. PAH oxidative loss was estimated as a first-order process  
438 using the model-predicted OH concentration immediately preceding particle-gas  
439 partitioning. Only seven new gas-phase concentration fields were added to the CTM;  
440 PAH reaction products were not tracked in the model, either as individual gas-phase  
441 species or as contributors to SOA.

442

443 Hydroxyl reaction rate constants were taken from the program AOPWIN which is part of  
444 the US EPA's EPI Suite (U.S. EPA, 2006). Measured constants are available for three  
445 low-molecular-weight PAHs considered here (phenanthrene, anthracene, fluoranthene)  
446 and these values were represented in AOPWIN. However, measurements for the  
447 remaining four PAHs are not available and the software predicted the same hydroxyl  
448 reaction rate constant of  $50 \times 10^{-12} \text{ cm}^3 \text{ molec}^{-1} \text{ s}^{-1}$  for these species.

449  
450 *2.1.3 Particle Representation of PAHs.* Seven additional particle species, each with 12  
451 size bins as in the original AURAMS configuration, were added to the model to represent  
452 the particle-bound PAH mass.

453  
454 *2.1.4 Particle/Gas Partitioning of PAHs.* A new algorithm was developed for  
455 AURAMS-PAH to account for the sorptive particle/gas partitioning of PAHs. It is fully  
456 adaptable to other semivolatile species with similar atmospheric partitioning behaviour to  
457 PAHs such as dioxins and furans, PCBs, and organochlorine pesticides. The partitioning  
458 of PAHs to airborne particles was assumed to be fully reversible.

459  
460 Two instantaneous equilibrium sorptive partitioning expressions were incorporated in the  
461 new partitioning subroutine. The first treated particle/gas partitioning as a Langmuirian  
462 adsorption process on a uniform particle surface (JP: Junge, 1977; Pankow, 1987). The  
463 model calculations began by adding the particulate PAH concentrations in all size bins  
464 ( $\Sigma C_p$ ) and the gas-phase PAH concentration ( $C_g$ ) to give a total PAH concentration  
465 ( $C_{TOT}$ ) for each species. An updated bulk particulate fraction ( $\phi$ ) was then assigned  
466 according to the first part of Eq. (1):

467

$$\phi = \frac{c \Sigma \theta}{c \Sigma \theta + p_L^0} = \frac{\Sigma C_p}{C_{TOT}}, \quad (1)$$

468  
469 where  $c$  is a constant set at  $0.173 \text{ J m}^{-2}$  (estimated from Figure 3 in Junge, 1977),  $\Sigma \theta$  is  
470 the total particle surface area concentration ( $\text{m}^2 \text{ m}^{-3}$ ) and  $p_L^0$  is the saturated vapour  
471 pressure of the sub-cooled liquid (Pa) taken from the temperature-dependent values  
472 measured by Offenbergl and Baker (1999; see Table S1.1). We have selected Junge's  
473 (1977) value of  $c$  over that estimated by Pankow (1987) since the latter was based on  
474 assumptions that have not been revisited in light of the numerous observations of PAH  
475 partitioning published since. The total particulate PAH concentrations dictated by  $\phi$  were  
476 then redistributed among the particle size bins by prorating to the proportion of total  
477 aerosol surface area concentration within each size bin. The redistributed gas-phase PAH  
478 concentration was determined by difference between  $C_{TOT}$  and  $\Sigma C_p$ .

479  
480 The second equilibrium partitioning expression available in the partitioning subroutine  
481 developed a partition coefficient ( $K_p$ ,  $\text{m}^3 \mu\text{g}^{-1}$ ) based on the contributions of two additive  
482 processes: absorption into particulate organic matter and adsorption onto particulate soot  
483 (DE: Dachs and Eisenreich, 2000)

484

$$K_p = 10^{-12} (1.5 f_{OC} / \rho_{oct} K_{OA} + f_{EC} K_{SA}) = \frac{(\sum C_p / C_{TSP})}{C_g}, \quad (2)$$

485

486 where  $\rho_{oct}$  is the bulk density of octanol ( $0.82 \text{ kg L}^{-1}$ ),  $f_{OC}$  is the organic carbon fraction  
 487 of the particulate matter (the 1.5 multiplier converts organic carbon to organic matter  
 488 which is assumed to be well-represented by octanol),  $K_{OA}$  is the octanol-air partition  
 489 coefficient (dimensionless),  $f_{EC}$  is the elemental carbon fraction of the particulate matter,  
 490  $K_{SA}$  is the soot-air partition coefficient ( $\text{L kg}^{-1}$ ),  $\sum C_p$  is the particulate PAH concentration  
 491 across all the size bins ( $\text{ng m}^{-3}$ ),  $C_{TSP}$  is the total particulate matter concentration ( $\mu\text{g m}^{-3}$ ),  
 492 and  $C_g$  is the gas-phase concentration ( $\text{ng m}^{-3}$ ).

493

494 Soot-air partition coefficients ( $K_{SA}, \text{L kg}^{-1}$ ) were estimated as the ratios of soot-water  
 495 ( $K_{SW}$ ) to air-water partition ( $K_{AW}$ ) coefficients since direct  $K_{SA}$  measurements are not  
 496 available for PAHs.  $K_{SW}$  values from Jonker and Koelmans (2002) were used in this  
 497 model. These values vary substantially (up to a factor of 47) between relevant soots for  
 498 each PAH considered here. Since a single  $K_{SW}$  was needed for each PAH in the model,  
 499 representative values were determined by weighting the reported  $K_{SW}$  values by the  
 500 contribution of their related combustion processes to the total emitted fine particulate  
 501 matter ( $\text{PM}_{2.5}$ ) used in the inventory of Galarneau et al. (2007). Temperature-dependent  
 502  $K_{AW}$  values were taken from Bamford et al. (1999).  $K_{OA}$  values were taken from the  
 503 temperature-dependent expressions determined by Odabasi et al. (2006).

504

505 PAH partition coefficients were calculated according to the first part of Eq. (2). By  
 506 determining the contribution of each size bin's organic matter and soot carbon to the  
 507 totals across all size bins, the total particulate PAH was apportioned to each size bin. For  
 508 example, if a total partition coefficient had contributions from the organic matter and soot  
 509 carbon of 20% and 80%, respectively, and size bin 1 held 10% of the total particulate  
 510 organic matter and 15% of the total soot carbon, the fraction of total particulate PAH  
 511 assigned to size bin 1 would be 14% (viz.,  $0.2 \times 0.1 + 0.8 \times 0.15$ ). Gas-phase  
 512 concentrations were then determined by difference between  $C_{TOT}$  and  $\sum C_p$ .

513

514 *2.1.5 Below-cloud (Precipitation) Scavenging.* Scavenging of gas and particle PAHs by  
 515 liquid precipitation was calculated as per Gong et al. (2006). Particle scavenging  
 516 assumed that particle-bound PAHs do not dissolve in falling rain; particle-bound PAHs  
 517 were thus treated as passive aerosol tracers. Snow scavenging of gaseous PAHs was not  
 518 considered in this version of AURAMS though particle-bound PAHs are scavenged by  
 519 snow in the model as passive components of airborne particles.

520

521 *2.1.6 Cloud Processing.* Cloud processing in the model was treated in a similar manner  
 522 to precipitation scavenging whereby gas-phase mass transfer to cloud water is species-  
 523 dependent, whereas particulate interactions with cloud droplets are only affected by the  
 524 presence of PAHs in terms of the size (mass and volume) that they represent as part of  
 525 the overall aerosol. Solid-phase densities used to relate aerosol PAH mass to volume  
 526 were taken from Mackay et al. (2006; see Table S1.1).

527

## 528 **2.2 Model Domain, Emissions, and Boundary Conditions**

529

530 The model domain included southern Canada and the continental USA (see Figure 1). It  
531 was run on a 42-km polar stereographic grid using off-line meteorology generated with  
532 the Global Environmental Multiscale numerical weather prediction model (GEM v 3.2.0:  
533 Côté et al., 1998a, b).

534

535 Emissions of PAHs were taken from the inventory of Galarneau et al. (2007) that had  
536 been updated from 2000 to 2002 and to which benzo[a]pyrene had been added using  
537 identical methods and data sources. As discussed in Galarneau et al. (2007), hourly PAH  
538 emissions fields were estimated with an emissions processing system using source-  
539 specific temporal profiles. The temporal profile library included 3020 month-of-year, 64  
540 day-of-week, and 2672 hour-of-day temporal profiles for Canada and 1500, 49, and 680  
541 analogous temporal profiles for the US. The overall temporal profile thus varies from  
542 grid cell to grid cell due to the different mixtures of source types found in each one.

543

544 All PAHs were emitted exclusively in the gas phase. Particle/gas partitioning took place  
545 at each 15-minute CTM time step according to the partitioning module described in  
546 Section 2.1.5. As mentioned in Section 2.1.2, no emissions of previously deposited  
547 PAHs were considered in this first-generation version of the model and the implications  
548 of this are discussed in Section 3.1.1. Emissions of SO<sub>2</sub>, NO<sub>x</sub>, NH<sub>3</sub>, CO, volatile organic  
549 compounds (VOCs), and particulate matter were derived using Environment Canada and  
550 US EPA databases and methods for the year 2002.

551

552 Initial PAH concentrations at all lateral boundaries were set to zero in anticipation of  
553 pronounced spatial gradients away from localised source regions. As a result, modelled  
554 concentrations in Mexico and near its border with the US are not expected to be reliable,  
555 particularly since PAH emissions from Mexico have not been included in the model.  
556 Model output along the northern edge of the domain over western Canada is similarly  
557 expected to be unreliable since emission sources are located close to the model boundary  
558 in that region. The development of representative non-zero boundary concentrations is  
559 anticipated as part of future model development.

560

### 561 **2.3 Evaluation Data**

562

563 Observational PAH data used for comparison with model output were collected from four  
564 measurement networks: NAPS (Canada), IADN (Canada-US), CARB (California), and  
565 Rio Tinto Alcan (Kitimat, British Columbia, Canada). The measurement stations are  
566 depicted in Figure 2 and described in Section 2 of the Supplementary Material.

567

568 Measurement data were available from a total of 45 stations, 23 in Canada and 22 in the  
569 USA, all of which collected samples integrated over periods of 24 hours. Particle/gas  
570 partitioning was assessed at eight stations, three in Canada and five in the USA, all of  
571 which were operated by IADN.

572

573 The IADN phase-distributed data were also combined to yield total concentrations.  
574 These combined IADN data, along with NAPS and Rio Tinto data, yielded a total of 28  
575 sites at which total PAH concentration for all the modelled PAHs could be assessed.



576 Particulate PAH measurements from the latter networks were determined from samples  
 577 of total suspended particles (TSP). CARB provided data for benzo[a]pyrene in particles  
 578 smaller than 2.5 µm in diameter (PM<sub>2.5</sub>) at a further 17 locations.

579  
 580 Four model grid squares (Kitimat, Toronto, Hamilton, and Montreal) contained two or  
 581 more measurement stations thus allowing for an assessment of the adequacy of modelling  
 582 all seven PAHs at 42-km grid spacing.

583

### 584 3. Results

585

#### 586 3.1 Total PAH Concentration

587

##### 588 3.1.1 Overall Spatiotemporal Domain

589

590 Total PAH concentration refers to the sum of the gas and particulate concentrations  
 591 whether these have been analysed together (e.g., NAPS) or separately (e.g., IADN). For  
 592 stations at which the gas and particle phases were analysed separately, a valid total  
 593 concentration was assumed to exist if at least one of the gas and particle phase  
 594 concentrations was greater than the detection limit. Non-detectable values were assumed  
 595 equal to zero for the calculation of total concentrations.

596

597 A representative plot of the spatial distribution of modelled annual average  
 598 concentrations is presented in Figure 1 for fluoranthene. The remaining PAHs show  
 599 similar spatial distributions and maps of their modelled concentrations are found in  
 600 Section 3 of the Supplementary Material. All the PAHs show spatial distributions of  
 601 their modelled concentrations that are consistent with regional dispersion of their  
 602 emissions as depicted in Galarnau et al. (2007).

603

604 A summary of annual mean modelled and measured values over the entire spatiotemporal  
 605 model domain is shown in Table 1. Only modelled values for which there was a  
 606 corresponding measurement were included.

607

608 **Table 1:** Summary of 2002 Annual Modelled and Measured Total PAH Concentration  
 609 Mean (Standard Deviation) Values (ng m<sup>-3</sup>)

610

PAH	Modelled – JP	Modelled - DE	Measured	n <sup>†</sup>
PHEN	12.75 (36.44)	12.76 (36.44)	36.06 (131.8)	790
ANTH	0.9123 (1.757)	0.9104 (1.759)	2.804 (11.56)	701
FLRT	6.781 (14.40)	6.888 (14.66)	9.179 (32.44)	789
PYR	5.727 (12.23)	6.009 (13.40)	5.733 (21.57)	785
BaA	1.227 (2.438)	1.328 (2.704)	1.326 (6.081)	610
C+T	1.511 (3.964)	1.473 (3.569)	3.303 (21.95)	721
BaP	1.173 (2.002)	1.424 (2.455)	0.9047 (3.238)	595

611 <sup>†</sup>n = number of modelled-measured data pairs

612

613 In comparing modelled results to measurements, the annual means were statistically  
 614 indistinguishable at the 95% confidence level for FLRT, PYR, BaA, and BaP (JP)  
 615 whereas they were statistically different for PHEN, ANTH, C+T, and BaP (DE). For

616 PHEN, ANTH, and C+T, modelled values were underestimated relative to measurements  
617 whereas they were overestimated for DE BaP.

618  
619 The model's temporal variability tended to be smaller than that of the corresponding  
620 measurements; the relative standard deviations of the measurements were 1.3 to 2.7 times  
621 greater than those of the modelled values. A similar observation has been made in the  
622 modelling of particulate matter with AURAMS and other regional air quality models  
623 (Solazzo et al., 2012) For PAHs, this effect was also seen by Matthias et al. (2009) who  
624 concluded that temporal variability in PAH emissions was not adequately represented by  
625 their inventory. This is a plausible contributing factor in the current study as well.  
626 Furthermore, meteorological parameters vary over a scale much finer than that used for  
627 regional air quality models. As a result, observed concentrations from point locations can  
628 be expected to exhibit greater variability than modelled concentrations determined for  
629 entire grid squares.

630  
631 Differences in mean modelled total concentrations between the two partitioning versions  
632 (JP and DE) were statistically indistinguishable at 95% significance despite the finding  
633 that the two BaP model results differed in their comparison to measured values. The  
634 latter anomaly indicates that the BaP distributions were close to the 95% confidence  
635 threshold. As a result, no conclusion can be drawn about which partitioning mechanism  
636 was superior in simulating overall total PAH concentrations. Phase partitioning of  
637 semivolatile organic compounds (SVOCs) is a major determinant of their potential for  
638 long-range transport (Bidleman, 1988), yet it does not appear to have a large effect on the  
639 simulation of their total concentrations at the regional scale. Model performance in  
640 simulating phase partitioning is discussed in Section 3.2.

641  
642 The model's performance was also more closely evaluated by examining the pertinent  
643 data distributions. Figure 3 depicts frequency distributions of the ratios of modelled-to-  
644 measured concentrations for all of the valid data pairs available for the model evaluation.  
645 Four PAH species (ANTH, FLRT, PYR, and C+T) yielded median values of the  
646 modelled-to-measured concentration ratio that were close to the ideal value of unity (1.1,  
647 1.1, 1.5, and 1.4, respectively). PHEN showed an overall tendency toward  
648 underestimation by the model (0.2), whereas BaA and BaP tended toward overestimation  
649 (3.2/3.5 and 3.0/3.5 JP/DE, respectively).

650  
651 BaA and BaP are reactive PAHs (e.g., Behymer and Hites, 1985; Pöschl et al., 2001;  
652 Kwamena et al., 2004; Esteve et al., 2006, Shiraiwa et al., 2009) and the exclusion of  
653 particle-bound reactions in this first-generation model may explain a portion of their  
654 overestimation in AURAMS-PAH as suggested in a comparable model for Europe  
655 (Matthias et al., 2009). However, BaP is subject to losses during sampling (Menichini,  
656 2009) and some portion of the apparent model overestimation may in fact be due to  
657 measured concentrations that are biased low since the samplers used were not equipped  
658 with oxidant denuders. This presents a priority for future research since many  
659 jurisdictions use BaP as an indicator PAH when setting air quality standards.

660  
661 As presented in Section 2.1.2, volatilisation of gaseous PAHs from surface compartments  
662 such as water and soil was not included in this first-generation version of AURAMS-

663 PAH. If such volatilisation were significant to the balance of PAHs in ambient air  
664 relative to the other processes simulated, one would expect an overall bias in model  
665 results whereby the most volatile PAHs, which are found predominantly in the gas phase,  
666 would be underestimated and the least volatile particulate species would be unaffected.  
667 Summary results provide indefinite evidence. Volatile PHENphenanthrene is  
668 systematically underestimated yet its similarly volatile isomer, ANTHanthracene, shows  
669 an ambiguous central tendency whereby its mean concentrations are underestimated by  
670 the model (Table 1) but its median concentrations are not (Figure 3). Less volatile but  
671 nonetheless predominantly gaseous FLRTfluoranthene and PYRpyrene show no tendency  
672 toward underestimation.

673  
674 Though results are equivocal on an annual basis, monthly patterns observed in the model  
675 output are consistent with the absence of a seasonal source (e.g., air-surface exchange).  
676 Volatilisation from a variety of environmental compartments is typically stronger in  
677 warmer periods than in cooler ones (e.g., Nelson et al., 1998; Smith et al., 2001; Motelay-  
678 Massei et al., 2005; Bozlaker et al., 2008; Wang et al., 2011). Figure 4 shows the  
679 monthly distribution of modelled-to-measured concentration ratios for PHEN and PYR.  
680 Both exhibit higher values in winter than in summer as do ANTH and FLRT whereas this  
681 seasonality is not observed for the higher molecular BaA, C+T or BaP (not shown).  
682 These findings are consistent with a missing volatilisation source that emits during  
683 warmer weather. However, other factors could also be involved including overestimated  
684 loss terms (e.g., oxidation, deposition) or underestimated emissions (e.g., forest fires)  
685 during warmer periods. The investigation of the relevant causes is a priority for future  
686 model development. Regardless of the causes, the seasonal effect on model output  
687 appears to be compounded by further, as yet unidentified factors whereby PHEN is  
688 underpredicted throughout the year and ANTH, FLRT and PYR are overpredicted  
689 through some seasons, potentially due to air-surface exchange that leads to net deposition  
690 during cooler months.

691  
692 ~~These results warrant further investigation but suggest that volatilisation of gaseous~~  
693 ~~PAHs from surface compartments may not be significant at the regional scale when~~  
694 ~~model results are compared to 24-hour measurements from predominantly urban~~  
695 ~~locations. This finding stands in contrast to the reported importance of air-surface~~  
696 ~~exchange at remote locations determined through global-scale modelling (Lammel et al.,~~  
697 ~~2009).~~

699 The range of modelled-to-measured concentration ratios shown in Figure 3 varied  
700 substantially by species. The ratios of 90<sup>th</sup> to 10<sup>th</sup> percentile values for PHEN, FLRT,  
701 PYR, BaA, and C+T spanned fewer than, or close to, two orders of magnitude (55, 59,  
702 67/68, 67/63, and 100/93, respectively). The ratio for BaP was larger (180/270) and that  
703 for ANTH was very large (5900/7400), with extreme values tending toward  
704 underestimation for the latter species. As seen with the comparison of means, the two  
705 partitioning parametrizations used by AURAMS-PAH led to similar model performance  
706 overall when considering the distribution of total PAH concentrations.

707  
708 Additional quantitative performance metrics are presented for the two particle/gas  
709 partitioning parametrizations in Tables S4.1 and S4.2 of the Supplementary Material.

710 Normalized mean bias and error have been included for completeness, but their utility in  
711 this evaluation is questionable given the large range of concentrations. Measured  
712 maximum to minimum concentration ratios range from 4.7E+06 (PYR) to  
713 1.3E+09/1.4E+09 (C+T). Therefore, the mean measured concentrations used to  
714 normalize the bias and error do not represent the dataset well.

715  
716 The correspondence between individual modelled-measured data pairs is weak as  
717 demonstrated by the low coefficients of determination, non-unity slopes, and high  
718 intercepts listed in Tables S4.1 and S4.2. However, the ability of the model to simulate  
719 observed concentrations within a certain tolerance is reasonable, especially when  
720 considering that PAHs are trace organic compounds subject to numerous sampling  
721 artefacts (McDow, 1999) and poor measurement precision (Galarneau, 2008).  
722 Depending on PAH species, 22-34% of modelled-measured data pairs fell within a factor  
723 of 2 of each other. This increased to 61-86% when considering a factor of 10. As a  
724 result, it can be stated with confidence that, on average, AURAMS-PAH was able to  
725 simulate atmospheric PAH concentrations in North America for rural to urban locations  
726 to the correct order of magnitude.

### 727 728 **3.1.2 Site-Specific Performance**

729  
730 Model performance was not spatially uniform. Figure 54 depicts the variation in  
731 distributions of individual modelled-to-measured concentration ratios across  
732 measurement sites for fluoranthene, the PAH species for which overall performance was  
733 best as determined by the median and spread in modelled-to-measured concentration  
734 ratios. Note that only JP partitioning values have been plotted since these are visually  
735 indistinguishable from those for DE partitioning.

736  
737 Of the 30 sites depicted in Figure 54 (CARB sites could not be considered since only  
738 benzo[a]pyrene was reported there), the median modelled-to-measured concentration  
739 ratio ranged from 0.061 (St. John's) to 4.0 (Hamilton – Confederation Park), whereas the  
740 median value for all sites was 1.1. The variability at individual sites is itself highly  
741 variable, with ratios of 90<sup>th</sup> to 10<sup>th</sup> percentile values of the modelled-to-measured  
742 concentration ratio ranging from 5.8 (Toronto – Junction Triangle) to 105,000 (Haul  
743 Road, near the Rio Tinto Alcan smelter in Kitimat, British Columbia). A low value of  
744 1.1 was observed for Saint John, but this was based on only two modelled-measured data  
745 pairs. Sixteen of the 30 sites (53%) had median modelled-to-measured ratios that fell  
746 within a factor of two of the median value for all sites.

747  
748 The other compounds varied spatially in a manner similar to fluoranthene with the  
749 following exceptions. ANTH exhibited atypically large underestimation at the three sites  
750 near the Rio Tinto Alcan smelter in Kitimat, suggesting that inaccurately low ANTH  
751 emissions are associated with the dominant source there. The reporting threshold for  
752 point-source ANTH emissions through the Canadian National Pollutant Release  
753 Inventory (NPRI) system is higher than the thresholds for other commonly-measured  
754 PAHs and no ANTH emissions were reported to the NPRI by Rio Tinto Alcan for 2002.  
755 The C+T performance at Jonquière, home to aluminum smelting facilities, suggests that  
756 reported emissions there are also too low. Emissions for other PAHs were reported from

757 this location for 2002 but not so for chrysene, which is called benzo[a]phenanthrene in  
 758 the NPRI.

759

### 760 3.1.3 Model Grid Squares Containing Multiple Measurement Sites

761

762 The smoother the spatial distribution of a pollutant, the coarser the model resolution that  
 763 can be used to simulate it. Four AURAMS-PAH model grid squares contain more than  
 764 one measurement site, thus allowing for an assessment of the 42-km spatial resolution  
 765 used for the evaluation runs. The multi-site grid squares are all located in Canada, and  
 766 from west to east, they encompass sites in Kitimat (2 sites), Hamilton (2), Toronto (3),  
 767 and Montreal (2) (see Tables S2.1 and S2.4).

768

769 Kitimat is a town 650 km northwest of Vancouver with approximately 9,000 residents  
 770 whose largest employer is the aluminum smelter complex operated by Rio Tinto Alcan  
 771 (District of Kitimat, 2009). Two measurement sites (Haul Road and Kitamaat Village)  
 772 are located in the same model grid square and a third site (Whitesail) lies in an adjacent  
 773 square even though it is only a few kilometers away. Hamilton is a city at the western  
 774 end of Lake Ontario that is known colloquially as the Steel Capital of Canada and had a  
 775 population of approximately 700,000 in 2010. It is part of the so-called “Golden  
 776 Horseshoe” conurbation at the western end of Lake Ontario whose 2010 population,  
 777 estimated as the sum of the populations of Oshawa, Toronto, Hamilton, and St.  
 778 Catharines-Niagara, was over 7 million (Statistics Canada, 2011). Toronto and Montreal  
 779 are the largest cities in Canada having 2010 populations of 5.7 and 3.9 million,  
 780 respectively.

781

782 Table 2 lists the variability in contemporaneously measured concentrations at the four  
 783 grid squares as represented by their coefficients of variation (COV). At any given site,  
 784 the average COVs for the different PAH species tend to be similar to each other.  
 785 Substantial differences exist between sites, however, particularly when grouping the  
 786 urban sites (Hamilton, Toronto, and Montréal) against the industrial site at Kitimat. This  
 787 is not unexpected. Urban areas include complex mixtures of point, area, and mobile  
 788 sources that are distributed over distances similar to the scale of the model. Kitimat  
 789 houses industrial operations within a relatively small area of otherwise rural land and  
 790 wilderness. Steep spatial gradients in pollutant concentrations are expected there as a  
 791 result.

792

793 **Table 2: Average Coefficient of Variation (%) between Contemporaneous**  
 794 **Measurements at Sites Falling Within the Same 42-km AURAMS-PAH Grid Square**

795

Station	PHEN	ANTH	FLRT	PYR	BaA	C+T	BaP	O <sub>3</sub> <sup>2</sup>	TSP
Kitimat	106	101	96.5	93.7	87.4	91.3	93.2	N/A	N/A
Hamilton	52.1	59.0	59.2	58.8	73.1	117	62.8	24.9	30.5
Toronto3 <sup>1</sup>	36.2	48.7	42.5	39.6	42.2	32.9	43.0	N/A	22.1
Toronto2 <sup>1</sup>	36.5	45.4	39.3	35.7	32.9	25.0	38.0	12.2	24.6
Montréal	49.2	52.9	45.8	44.6	55.2	55.3	51.6	35.3	29.0

796

797 <sup>1</sup> Toronto3 includes data from all three Toronto measurement sites. Toronto2 includes only data from the Gage Institute and Judson &  
 798 Etona because O<sub>3</sub> data were not available from Junction Triangle.

799

<sup>2</sup> Ozone data have been aggregated to 24-hour concentrations contemporaneous with PAH measurements.

800

801 The COVs for ozone and total suspended particles (TSP) have also been included in  
802 Table 2 as comparative gaseous and particulate pollutants, respectively. Both vary less  
803 between sites in the same grid square than do PAHs. Ozone and a portion of TSP are  
804 secondary pollutants created by the mixing and reaction of precursor compounds. The  
805 atmospheric residence times required for their creation is consistent with a smoothing of  
806 the spatial variability in their concentrations though ozone variability is further  
807 complicated by reactions with  $\text{NO}_x$  near emissions from mobile sources. Conversely,  
808 unsubstituted PAHs are primary pollutants whose concentrations would be expected to  
809 vary in space over a finer resolution when multiple sources are found close by.

810

811 The results presented above suggest that a 42-km spatial resolution is not sufficiently fine  
812 to represent PAH concentrations in areas close to sources such as cities and industrial  
813 areas if an average model accuracy better than an order of magnitude is desired.  
814 AURAMS modelling of fine particulate matter has shown substantial improvement when  
815 grid spacing has been reduced to 2.5 km (Stroud et al., 2011), and similar results can be  
816 expected for the modelling of PAHs. No 42-km model grid squares in rural or  
817 background areas away from sources contain multiple measurement stations and, as a  
818 result, a comparison cannot be made for these areas. However, it is expected that spatial  
819 variation in PAH concentrations will be less in such areas and, as such, a 42-km  
820 resolution model may be sufficient there.

821

## 822 **3.2 Particle/Gas Partitioning**

823

824 As noted in Section 3.1, the choice of partitioning expression (JP or DE) had little effect  
825 on the simulation of total PAH concentrations. This implies that the partitioning from  
826 each approach is sufficiently similar that regional-scale differences in removal rates  
827 between gaseous and particulate PAHs have little effect. However, differences between  
828 the two expressions with respect to simulating phase-resolved concentrations were noted.

829

### 830 **3.2.1 Overall Spatiotemporal Domain**

831

832 | Figure 65 shows frequency distributions of the ratios of individual modelled-to-measured  
833 particulate fraction for all data pairs available to the model evaluation. Note that only the  
834 eight IADN stations are included since the gas and particle phases are analysed separately  
835 only at those sites.

836

837 | Figure 65 shows that PAH particulate fraction is underestimated for all species except  
838 BaP. The degree of underestimation decreases with increasing molecular weight. The  
839 particulate fractions of volatile PHEN and ANTH ( $178 \text{ g mol}^{-1}$ ) are underestimated by  
840 approximately two orders of magnitude whereas equipartitioning BaA and C+T ( $228 \text{ g}$   
841  $\text{mol}^{-1}$ ) have particulate fractions that are underestimated by only a factor of two. A  
842 similar pattern appears when examining the partition coefficient,  $K_p$  (not shown).

843

844 For all species other than BaP, Dachs-Eisenreich partitioning performs slightly better  
845 than Junge-Pankow partitioning in simulating measured particulate fractions. The all-site  
846 median particulate fraction simulated using DE is between 1.1 (PYR) and 2.9 (ANTH)

847 times higher than that using JP. However, the performance of the partitioning  
848 expressions is highly dependent on the physico-chemical property values used. For  
849 example, estimated soot-air partition coefficients vary by more than an order of  
850 magnitude (Galarneau et al., 2006) and translate directly to variations in predicted  
851 partitioning by the Dachs-Eisenreich expression. For Junge-Pankow partitioning, the  
852 value of the constant,  $c$ , in Eq. 1 and the estimation of aerosol surface area also introduce  
853 uncertainties. A full analysis of the sensitivity of modelled partitioning is beyond the  
854 scope of this paper and is explored in a separate publication (Galarneau et al., in prep.).  
855

### 856 3.2.2 Site-Specific Performance

857  
858 As was the case for total concentration, there is substantial variability in the simulation of  
859 partitioning between sites. Figure 76 shows the variation in frequency distribution of  
860 individual modelled-to-measured particulate fraction for fluoranthene using Dachs-  
861 Eisenreich partitioning. Model performance for particulate fraction simulation is better at  
862 urban (Chicago) or urban-influenced (Sturgeon Point, Egbert) sites than at those that are  
863 remote (Eagle Harbor). An analysis of measured partitioning at IADN stations  
864 (Galarneau et al., 2006) found that the proportionality between partitioning and volatility  
865 varied between sites, and in some cases, over the annual cycle. Volatility is included in  
866 both the JP (through  $p_L^0$ ) and DE (through  $K_{OA}$  and  $K_{SA}$ ) partitioning expressions and the  
867 proportionality between it and partitioning magnitude is much smaller in model outputs  
868 than in measurements. As noted earlier, factors involved in the performance of model  
869 partitioning such as modelled particulate matter concentration and composition are  
870 explored in a separate publication (Galarneau et al., in prep.)  
871

## 872 4. Conclusions

873  
874 This study described the first known modelling results for atmospheric PAHs at the  
875 regional scale over North America. Predictions from the AURAMS-PAH model were  
876 compared to roughly 5,000 24-hour average PAH measurements from 45 sites, eight of  
877 which also provided data on particle/gas partitioning which had been modelled using two  
878 different partitioning schemes.  
879

880 The evaluation of the model is key to determining its potential utility as an input for  
881 estimating the impacts of PAH inhalation exposure on human health. Annual average  
882 modelled total (gas + particle) concentrations were statistically indistinguishable from  
883 measured values for fluoranthene, pyrene and benz[a]anthracene, indicating the model's  
884 potential utility for providing inputs to health impact estimation for these species. The  
885 model annual average concentrations for phenanthrene, anthracene and  
886 chrysene+triphenylene were biased low. For these species, the negative bias would have  
887 to be considered if used as inputs to human health impact estimates as the model in its  
888 present form underestimates long-term exposure.  
889

890 The utility of the model for prediction purposes may also be considered on a day-to-day  
891 basis though this is less relevant to the chronic health effects associated with carcinogenic  
892 PAHs. The model simulated total PAH concentrations to the correct order of magnitude  
893 64-86% of the time. That level of accuracy must be considered when assessing human

894 health impacts; annual exposure estimates are likely of more utility with the model in its  
895 current state.

896

897 The partitioning approach chosen did not have a significant impact on the model results  
898 for total concentrations though differences resulting from the choice of parametrization  
899 approached the 95% significance level for benzo[a]pyrene. At this time, neither of the  
900 two approaches used here provided a clear advantage for simulation accuracy of total  
901 concentrations.

902

903 As a first work of this nature, the analysis has suggested several avenues for further  
904 model development and improvement. Improved temporal emissions estimates for PAHs  
905 are key to improving model simulations of these species; simulated PAHs showed less  
906 temporal variability than the measurements. The reactions of particulate PAH species  
907 with atmospheric oxidants should [be](#) given further consideration since the more reactive  
908 species were overestimated in the current model. [The addition of an air-surface exchange  
909 parametrisation should be evaluated as a potential response to the seasonally varying  
910 prediction capability of the model for the most volatile compounds.](#) Model resolution has  
911 been shown to be a key factor in improving air pollution estimates in areas with high  
912 human exposures. While the 42-km horizontal grid spacing used in this study is finer  
913 than that used in global models, it was insufficient to capture the distribution of  
914 concentrations in densely populated areas. A more detailed analysis of the factors  
915 influencing modelled particle/gas partitioning is needed to improve the distribution of  
916 PAHs between the gas and particle phases in the atmosphere given that both partitioning  
917 schemes used here showed increasing negative biases for particle-bound PAH  
918 concentrations of increasing volatility.

919

## 920 **Acknowledgements**

921

922 The authors would like to acknowledge the contributions of the AURAMS team at  
923 Environment Canada, in particular Balbir Pabla, Craig Stroud, Wanmin Gong, and  
924 Sunling Gong, as well as Sylvie Gravel. They thank Philip Cheung, ~~and~~ Keith Wong  
925 [and Trisha Mahtani](#) for their [assistance in efforts in](#) generating [some of the figures](#)  
926 [herein](#) ~~the maps of model output PAH concentrations~~. They also thank Nathalie Mayrand  
927 (Rio Tinto Alcan) [and the California Air Resources Board](#) for sharing measurement data  
928 from the Kitimat area [and California, respectively](#). Finally, the authors thank Terry  
929 Bidleman and Miriam Diamond for their guidance and support at the outset of this  
930 project.

931

932



933 **References**

934

935 Aulinger, A., Matthias, V., and Quante, M.: Introducing a partitioning mechanism for  
936 PAHs into the Community Multiscale Air Quality modeling system and its application to  
937 simulating the transport of benzo[a]pyrene over Europe, *J. Appl. Met. Clim.*, 46, 1718-  
938 1730, 2007.

939

940 Bamford, H.A., Poster, D.L., and Baker, J.E.: Temperature dependence of Henry's Law  
941 constants of thirteen polycyclic aromatic hydrocarbons between 4°C and 31°C, *Environ.*  
942 *Toxicol. Chem.*, 18, 1905-1912, 1999.

943

944 Behymer, T.D. and Hites, R.A.: Photolysis of polycyclic aromatic hydrocarbons adsorbed  
945 on simulated atmospheric particulates, *Environ. Sci. Technol.*, 19, 1004-1006, 1985.

946

947 Bidleman, T.F.: Atmospheric processes: Wet and dry deposition of organic compounds  
948 are controlled by their vapor-particle partitioning, *Environ. Sci. Technol.*, 22, 361-367,  
949 1988.

950

951 Bieser, J., Aulinger, A., Matthias, V., and Quante, M.: Impact of emission reductions  
952 between 1980 and 2020 on atmospheric benzo[a]pyrene concentrations over Europe.  
953 *Water Air Soil Pollut.*, 223, 1393-1414, 2012.

954

955 Blanchard, P., Audette, C.V., Hulting, M.L., Basu, I., Brice, K.A., Backus, S.M.,  
956 Dryfhout-Clark, H., Froude, F., Hites, R.A., Neilson, M., and Wu, R.: Atmospheric  
957 deposition of toxic substances to the Great Lakes: IADN results through 2005, ISBN  
958 En56-146/2005E, Environment Canada and US EPA, Toronto, 2008.

959

960 [Bozlaker, A., Muezzinoglu, A., and Odabasi, M.: Atmospheric concentrations, dry](#)  
961 [deposition and air-soil exchange of polycyclic aromatic hydrocarbons \(PAHs\) in an](#)  
962 [industrial region in Turkey, \*J. Haz. Mat.\*, 153, 1093-1102, 2008.](#)

963

964 €

965 Côté, J., Desmarais, J.-G., Gravel, S., Méthot, A., Patoine, A., Roch, M., and Staniforth,  
966 A.: The operational CMC-MRB Global Environment Multiscale (GEM) model: Part I.  
967 Design considerations and formulation, *Mon. Weather Rev.*, 126, 1373-1395, 1998.

968

969 Côté, J., Desmarais, J.-G., Gravel, S., Méthot, A., Patoine, A., Roch, M., and Staniforth,  
970 A.: The operational CMC-MRB Global Environment Multiscale (GEM) model: Part II.  
971 Results, *Mon. Weather Rev.*, 126, 1397-1418, 1998.

972

973 [Cousins, I.T., and Jones, K.C.: Air-soil exchange of semivolatile organic compounds](#)  
974 [\(SOCs\) in the UK, \*Environ. Poll.\*, 102, 105-118, 1998.](#)

975

976 Dachs, J. and Eisenreich, S.J.: Adsorption onto aerosol soot carbon dominates gas-  
977 particle partitioning of polycyclic aromatic hydrocarbons, *Environ. Sci. Technol.*, 34,  
978 3690-3697, 2000.

979

Formatted: Font: (Default) Times New Roman, 12 pt, Font color: Auto

Formatted: Font: (Default) Times New Roman, 12 pt, Font color: Auto

Formatted: Font: (Default) Times New Roman, 12 pt, Font color: Auto

Formatted: Font: (Default) Times New Roman, 12 pt, Font color: Auto

Formatted: Font: (Default) Times New Roman, 12 pt, Font color: Auto

Formatted: Font: (Default) Times New Roman, 12 pt, Font color: Auto

980 Diamond, M.L., Gingrich, S.E., Fertuck, K., McCarry, B.E., Stern, G.A., Billeck, B.,  
981 Grift, B., Brooker, D., and Yager, T.D.: Evidence for organic film on an impervious  
982 urban surface: characterization and potential teratogenic effects, *Environ. Sci. Technol.*,  
983 34, 2900-2908, 2000.

984  
985 District of Kitimat: Kitimat, British Columbia Community Profile, District of Kitimat,  
986 B.C. 2009. <http://www.kitimat.ca/assets/Residents/PDFs/community-profile.pdf>  
987

988 Environment Canada and Health Canada: Canadian Environmental Protection Act:  
989 Priority Substances List Assessment Report: Polycyclic Aromatic Hydrocarbons,  
990 Government of Canada, Ottawa, ON, Cat. No. En40-215/42E, 66 pp., 1994.

991  
992 Environment Canada: Historical emission trends for benzo[a]pyrene in Canada  
993 (kilograms), [http://www.ec.gc.ca/pdb/websol/emissions/ap/ap\\_result\\_e.cfm?year=1985-](http://www.ec.gc.ca/pdb/websol/emissions/ap/ap_result_e.cfm?year=1985-2007&substance=bap&location=CA&sector=&submit=Search)  
994 [2007&substance=bap&location=CA&sector=&submit=Search](http://www.ec.gc.ca/pdb/websol/emissions/ap/ap_result_e.cfm?year=1985-2007&substance=bap&location=CA&sector=&submit=Search), last access: 28 September  
995 2012.  
996

997 Esteve, W., Budzinski, H. and Villenave, E.: Relative rate constants for the  
998 heterogeneous reactions of NO<sub>2</sub> and OH radicals with polycyclic aromatic hydrocarbons  
999 adsorbed on carbonaceous particles. Part 2: PAHs adsorbed on diesel particulate exhaust  
1000 SRM 1650a, *Atmos. Environ.*, 40, 201-211, 2006.

1001  
1002 Finizio, A., Mackay, D., Bidleman, T. and Harner, T.: Octanol-air partition coefficient as  
1003 a predictor of partitioning of semi-volatile organic chemicals to aerosols, *Atmos.*  
1004 *Environ.*, 31, 2289-2296, 1997.

1005  
1006 Friedman, C.L. and Selin, N.E.: Long-range atmospheric transport of polycyclic aromatic  
1007 hydrocarbons: a global 3-D model analysis including evaluation of arctic sources,  
1008 *Environ. Sci. Technol.*, 46, 9501-9510, 2012.

1009  
1010 Galarneau, E. Source specificity and atmospheric processing of airborne PAHs:  
1011 implications for source apportionment, *Atmos. Environ.*, 42, 8139-8149, 2008.

1012  
1013 Galarneau, E., Bidleman, T.F., and Blanchard, P.: Seasonality and interspecies  
1014 differences in particle/gas partitioning of PAHs observed by the Integrated Atmospheric  
1015 Deposition Network (IADN), *Atmos. Environ.*, 40, 182-197, 2006.

1016  
1017 Galarneau, E. and Dann, T.: Air toxics in Canada (ATiC): preliminary scoping report,  
1018 Environment Canada, Toronto, ON, 24 pp., 2011.

1019  
1020 Galarneau, E. et al.: Evaluation of particle/gas partitioning in a regional air quality model  
1021 (AURAMS-PAH), in preparation.

1022  
1023 Galarneau, E., Makar, P.A., Sassi, M., and Diamond, M.L.: Estimation of atmospheric  
1024 emissions of six semivolatile polycyclic aromatic hydrocarbons in southern Canada and  
1025 the United States by use of an emissions processing system, *Environ. Sci. Technol.*, 41,  
1026 4205-4213, 2007.

1027  
1028 Gong, S. L., Barrie, L.A., Blanchet, J.-P., von Salzen, K., Lohmann, U., Lesins, G.,  
1029 Spacek, L., Zhang, L.M., Girard, E., Lin, H., Leaitch, R., Leighton, H., Chylek, P., and  
1030 Huang, P.: Canadian Aerosol Module: A size-segregated simulation of atmospheric  
1031 aerosol processes for climate and air quality models. 1. Module development, *J. Geophys.*  
1032 *Res.*, 108, 4007, doi:10.1029/2001JD002002, 2003a.

1033  
1034 Gong, S. L., Barrie, L. A., and Lazare, M.: Canadian Aerosol Module (CAM): A size-  
1035 segregated simulation of atmospheric aerosol processes for climate and air quality models  
1036 2. Global sea-salt aerosol and its budgets, *J. Geophys. Res.*, 107, 4779,  
1037 doi:10.1029/2001JD002004, 2003b.

1038  
1039 Gong, W., Dastoor, A.P., Bouchet, V.S., Gong, S., Makar, P.A., Moran, M.D., Pabla, B.,  
1040 Ménard, S., Crevier, L.-P., Cousineau, S., and Venkatesh, S.: Cloud processing of gases  
1041 and aerosols in a regional air quality model (AURAMS), *Atmos. Res.*, 82, 248-275, 2006.

1042  
1043 Gusev, A.; Dutchak, S., Rozovskaya, O., Shatalov, V., Sokovykh, V., Vulykh, N., Aas,  
1044 W., Breivik, K.: Persistent organic pollutants in the environment, EMEP Status Report  
1045 3/2011, NILU and MSC-East, 2011.

1046  
1047 Hafner, W.D., Carlson, D.L., and Hites, R.A.: Influence of local human population on  
1048 atmospheric polycyclic aromatic hydrocarbon concentrations, *Environ. Sci. Technol.*, 39,  
1049 7374-7379, 2005.

1050  
1051 Halsall, C.J., Sweetman, A.J., Barrie, L.A., and Jones, K.C.: Modelling the behaviour of  
1052 PAHs during atmospheric transport from the UK to the Arctic, *Atmos. Environ.*, 35, 255-  
1053 267, 2001.

1054  
1055 Hoff, R.M., Strachan, W.M.J., Sweet, C.W., Chan, C.H., Shackleton, M., Bidleman, T.F.,  
1056 Brice, K.A., Burniston, D.A., Cussion, S., Gatz, D.F., Harlin, K., and Schroeder, W.H.:  
1057 Atmospheric deposition of toxic chemicals to the Great Lakes: a review of data through  
1058 1994, *Atmos. Environ.*, 30, 3505-3527, 1996.

1059  
1060 Hung, H., Blanchard, P., Halsall, C.J., Bidleman, T.F., Stern, G.A., Felin, P., Muir,  
1061 D.C.G., Barrie, L.A., Jantunen, L.M., Helm, P.A., Ma, J., and Konoplev, A.: Temporal  
1062 and spatial variabilities in atmospheric polychlorinated biphenyls (PCBs), organochlorine  
1063 (OC) pesticides and polycyclic aromatic hydrocarbons (PAHs) in the Canadian Arctic:  
1064 results from a decade of monitoring, *Sci. Tot. Environ.*, 342, 119-144, 2005.

1065  
1066 Inomata, Y., Kajino, M., Sato, K., Ohara, T., Kurokawa, J.-I., Ueda, H., Tang, N.,  
1067 Hayakawa, K., Ohizumi, T., and Akimoto, H.: Emission and atmospheric transport of  
1068 particulate PAHs in Northeast Asia, *Environ. Sci. Technol.*, 46, 4941-4949, 2012.

1069  
1070 International Agency for Research on Cancer: IARC Monographs on the Evaluation of  
1071 Carcinogenic Risks to Humans: VOLUME 92: Some Non-heterocyclic Polycyclic  
1072 Aromatic Hydrocarbons and Some Related Exposures, IARC, Lyon, France, 2010.

1073  
1074 Jonker, M.T.O. and Koelmans, A.A.: Sorption of polycyclic aromatic hydrocarbons and  
1075 polychlorinated bipheyls to soot and soot-like materials in the aqueous environment:  
1076 mechanistic considerations, *Environ. Sci. Technol.*, 36, 3725-3734, 2002.  
1077  
1078 Jones, K.C.: Observations on long-term air-soil exchange of organic contaminants,  
1079 *Environ. Sci. & Pollut. Res.*, 1, 172-177, 1994.  
1080  
1081 Junge, C.E.: Basic considerations about trace constituents in the atmosphere as related to  
1082 the fate of global pollutants, in: *Fate of Pollutants in the Air and Water Environments*,  
1083 Suffet, I.H. (Ed.) Wiley, New York, 7-25, 1977.  
1084  
1085 Kelly, F.J. and Fussell, J.: Review: Size, source and chemical composition as  
1086 determinants of toxicity attributable to ambient particulate matter, *Atmos. Environ.*, 60,  
1087 504-526, 2012.  
1088  
1089 Kelly, J., Makar, P.A., and Plummer, D.A.: Projections of mid-century summer air-  
1090 quality for North America: effects of changes in climate and precursor emissions,  
1091 *Atmos. Chem. Phys.*, 12, 5367-5390, 2012.  
  
1092 Kwamena, N.-O.A., Thornton, J.A., and Abbatt, J.P.D.: Kinetics of surface-bound  
1093 benzo[a]pyrene and ozone on solid organic and salt aerosols, *J. Phys. Chem. A*, 108,  
1094 11626-11634, 2004.  
  
1095  
1096 Lammel, G., Sehili, A.M., Bond, T.C., Feichter, J., and Grassl, H.: Gas/particle  
1097 partitioning and global distribution of polycyclic aromatic hydrocarbons: a modelling  
1098 approach, *Chemosphere*, 76, 98-106, 2009.  
1099  
1100 Lang, C., Tao, S., Liu, W., Zhang, Y., and Simonich, S.: Atmospheric transport and  
1101 outflow of polycyclic aromatic hydrocarbons from China, *Environ. Sci. Technol.*, 42,  
1102 5196-5201, 2008.  
1103  
1104 Lang, C., Tao, S., Zhang, G., Fu, J., and Simonich, S.: Outflow of polycyclic aromatic  
1105 hydrocarbons from Guangdong, southern China, *Environ. Sci. Technol.*, 41, 8370-8375,  
1106 2007.  
1107  
1108 Liu, S., Tao, S., Liu, W., Liu, Y., Dou, H., Zhao, J., Wang, L., Wang, J., Tian, Z., and  
1109 Gao, Y.: Atmospheric polycyclic aromatic hydrocarbons in north China: a winter-time  
1110 study, *Environ. Sci. Technol.*, 41, 8256-8261, 2007.  
1111  
1112 Mackay, D., Shiu, W.Y., Ma, K.-C., and Lee, S.C: *Handbook of physical-chemical*  
1113 *properties and environmental fate for organic chemicals*. Vol. 1: Introduction and  
1114 hydrocarbons. Taylor and Francis, Boca Raton, FL, USA, 2006.  
1115  
1116 Makar, P.A., Zhang, J., Gong, W., Stroud, C., Sills, D., Hayden, K.L., Brook, J., Levy, I.,  
1117 Mihele, C., Moran, M.D., Tarasick, D.W., and He, H.: Mass tracking for chemical

1118 analysis: the causes of ozone formation in southern Ontario during BAQS-Met 2007,  
1119 Atmos. Chem. Phys., 10, 11151-11173, 2010.  
1120  
1121 Matthias, V., Aulinger, A., and Quante, M.: CMAQ simulations of the benzo[a]pyrene  
1122 distribution over Europe for 200 and 2001, Atmos. Environ., 43, 4078-4086, 2009.  
1123  
1124 McDow, S.R.: Sampling artefact errors in gas/particle partitioning measurements, in: Gas  
1125 and Particle Phase Measurements of Atmospheric Organic Compounds, Lane, D.A. (Ed.),  
1126 Gordon and Breach Science Publishers, Canada, 105-126, 1999.  
1127  
1128 McKeen, S., Chung, S.H., Wilczak, J., Grell, G., Djalalova, I., Peckham, S., Gong, W.,  
1129 Bouchet, V., Moffet, R., Tang, Y., Carmichael, G.R., Mathur, R., and Yu, S.: Evaluation  
1130 of several real-time PM<sub>2.5</sub> forecast models using data collected during the  
1131 ICARTT/NEAQS 2004 field study, J. Geophys. Res., 112, D10S20,  
1132 doi:10.1029/2006JD007608, 2007.  
1133  
1134 Menichini, E.: On-filter degradation of particle-bound benzo[a]pyrene by ozone during  
1135 air sampling: a review of the experimental evidence of an artefact, Chemosphere, 77,  
1136 1275-1284, 2009.  
1137  
1138 [Motelay-Massei, A., Harner, T., Shoeib, M., Diamond, M., Stern, G., and Rosenberg, B.:](#)  
1139 [Using Passive Air Samplers To Assess Urban–Rural Trends for Persistent Organic](#)  
1140 [Pollutants and Polycyclic Aromatic Hydrocarbons. 2. Seasonal Trends for PAHs, PCBs,](#)  
1141 [and Organochlorine Pesticides, 39, 5763-5773, 2005.](#)  
1142  
1143 [Nelson, E.D., McConnell, L.L., and Baker, J.E.: Diffusive exchange of gaseous](#)  
1144 [polycyclic aromatic hydrocarbons and polychlorinated biphenyls across the air-water](#)  
1145 [interface of the Chesapeake Bay, Environ. Sci. Technol., 32, 912-919, 1998.](#)  
1146  
1147 Odabasi, M., Cetin, E., and Sofuoglu, A.: Determination of octano-air partition  
1148 coefficients and supercooled liquid vapour pressures of PAHs as a function of  
1149 temperature: application to gas-particle partitioning in an urban atmosphere, Atmos.  
1150 Environ., 40:6615-6625, 2006.  
1151  
1152 Offenberg, J.H. and Baker, J.E.: Aerosol size distributions of polycyclic aromatic  
1153 hydrocarbons in urban and over-water atmospheres, Environ. Sci. Technol., 33, 3324-  
1154 3331, 1999.  
1155  
1156 Pankow, J.F.: Review and comparative analysis of the theories on partitioning between  
1157 the gas and aerosol particulate phases in the atmosphere, Atmos. Environ., 21, 2275-  
1158 2283, 1987.  
1159  
1160 Pöschl, U., Letzel, T., Schauer, C., and Niessner, R.: Interaction of ozone and water  
1161 vapor with spark discharge soot aerosol particles coated with benzo[a]pyrene: O<sub>3</sub> and

Formatted: Font: 12 pt, Not Bold

Formatted: Font: 12 pt, Not Bold

1162 H<sub>2</sub>O adsorption, benzo[a]pyrene degradation, and atmospheric implications, *J. Phys.*  
1163 *Chem. A*, 105, 4029-4041, 2001.

1164  
1165 Prevedouros, K., Jones, K.C., and Sweetman, A.J.: Modelling the atmospheric fate and  
1166 seasonality of polycyclic aromatic hydrocarbons in the UK, *Chemosphere*, 56, 195-208,  
1167 2004.

1168  
1169 Prevedouros, K., Palm-Cousins, A., Gustafsson, Ö., and Cousins, I.T.: Development of a  
1170 black carbon-inclusive multi-media model: application for PAHs in Stockholm,  
1171 *Chemosphere*, 70, 607-615, 2008.

1172  
1173 Reid, R.C., Prausnitz, J.M., and Poling, B.E.: The properties of gases and liquids.  
1174 McGraw-Hill, Toronto, 1987.

1175  
1176 Sehili, A.M. and Lammel, G.: Global fate and distribution of polycyclic aromatic  
1177 hydrocarbons emitted from Europe and Russia, *Atmos. Environ.*, 41, 8301-8315, 2007.

1178  
1179 Shatalov, V., Gusev, A., Dutchak, S., Holoubek, I., Mantseva, E., Tozovskaya, O.,  
1180 Sweetman, A., Strukov, B., and Vulykh, N.: Modelling of POP contamination in  
1181 European region: evaluation of the model performance, EMEP/MS-CHEM Technical Report  
1182 7/2005, 2005.

1183  
1184 Shiraiwa, M., Garland, R.M., and Pöschl, U.: Kinetic double layer model of aerosol  
1185 surface chemistry and gas-particle interactions (K2-SURF): degradation of polycyclic  
1186 aromatic hydrocarbons exposed to O<sub>3</sub>, NO<sub>2</sub>, H<sub>2</sub>O, OH and NO<sub>3</sub>, *Atmospheric*  
1187 *Chemistry and Physics*, 9, 9571-9586, 2009.

1188  
1189 [Smith, K.E.C., Thomas, G.A., and Jones, K.C.: Seasonal and species differences in the](#)  
1190 [air-pasture transfer of PAHs, \*Environ. Sci. Technol.\*, 35, 2156-2165, 2001.](#)

1191  
1192 Smyth, S.C., Jiang, W., Roth, H., Moran, M.D., Makar, P.A., Yang, F., Bouchet, V.S.,  
1193 and Landry, H.: A comparative performance evaluation of the AURAMS and CMAQ air-  
1194 quality modelling systems, *Atmos. Environ.*, 43, 1059-1070, 2009.

1195  
1196 Solazzo, E., Bianconi, R., Vautard, R., Appel, K.W., Moran, M.D., Hogrefe, C.,  
1197 Bessagnet, B., Brandt, J., Christensen, J.H., Chemel, C., Coll, I., Denier van der Gon, H.,  
1198 Ferreira, J., Forkel, R., Francis, X.V., Grell, G., Grossi, P., Hansen, A.B., Jeričević, A.,  
1199 Kraljević, L., Miranda, A.I., Nopmongkol, U., Pirovano, G., Prank, M., Riccio, A.,  
1200 Sartelet, K.N., Schaap, M., Silver, J.D., Sokhi, R.S., Vira, J., Werhahn, J., Wolke, R.,  
1201 Yarwood, G., Zhang, J., Rao, S.T., and Galmarini, S.: Model evaluation and ensemble  
1202 modelling of surface-level ozone in Europe and North America in the context of  
1203 AQMEII. *Atmos. Environ.*, 53, 60-74, 2012.

1204  
1205 Statistics Canada: Population of census metropolitan areas,  
1206 <http://www40.statcan.ca/101/cst01/demo05a-eng.htm>, last access: 25 August 2011.

1207

1208 Stroud, C., Makar, P.A., Moran, M.D., Gong, W., Gong, S., Zhang, J., Hayden, K.,  
1209 Mihele, C., Brook, J.R., Abbatt, J.P.D., and Slowik, J.G.: Impact of model grid spacing  
1210 on regional- and urban- scale air quality predictions of organic aerosol, Atmos. Chem.  
1211 Phys., 11, 3107-3118, 2011.

1212  
1213 U.S. E.P.A.: Estimation program interface (EPI) suite.,  
1214 <http://www.epa.gov/opptintr/exposure/pubs/episuite.htm>, last access: 2 June 2006.

1215  
1216 U.S. E.P.A.: The Clean Air Act Amendments of 1990 List of Hazardous Air Pollutants.,  
1217 <http://www.epa.gov/ttnatw01/orig189.html>, last access: 28 September 2012.

1218  
1219 U.S. E.P.A.: TRI Explorer Web Tool,  
1220 [http://iaspub.epa.gov/triexplorer/tri\\_release.chemical](http://iaspub.epa.gov/triexplorer/tri_release.chemical), last access: 28 September 2012.

1221  
1222 US EPA: National-scale air toxics assessment (NATA). Summary of results for the 2005  
1223 national-scale assessment., [http://www.epa.gov/ttn/atw/nata2005/05pdf/sum\\_results.pdf](http://www.epa.gov/ttn/atw/nata2005/05pdf/sum_results.pdf),  
1224 last access: 28 September 2012.

1225  
1226 Van Jaarsveld, J.A., Van Pul, W.A.J., and De Leeuw, F.A.A.M.: Modelling transport and  
1227 deposition of persistent organic pollutants in the European region, Atmos. Environ., 31,  
1228 1011-1024, 1997.

1229  
1230 [Wang, W., Simonich, S., Giri, B., Chang, Y., Zhang, Y., Jia, Y., Tao, S., Wang, R.,](#)  
1231 [Wang, B., Li, W., Cao, J., Lu, X.: Atmospheric concentrations and air–soil gas exchange](#)  
1232 [of polycyclic aromatic hydrocarbons \(PAHs\) in remote, rural village and urban areas of](#)  
1233 [Beijing–Tianjin region, North China, Sci. Tot. Environ., 409, 2942-2950, 2011.](#)

1234  
1235 Yaffe, D., Cohen, Y., Arey, J., and Grosovsky, A.J.: Multimedia analysis of PAHs and  
1236 nitro-PAH daughter products in the Los Angeles Basin, Risk Analysis, 21, 275-294,  
1237 2001.

1238  
1239 Zhang, L., Moran, M.D., Makar, P.A., Brook, J.R., and Gong, S.: Modelling gaseous dry  
1240 deposition in AURAMS: an unified regional air-quality modelling system, Atmos.  
1241 Environ., 36, 537-560, 2002.

1242  
1243 Zhang, Y., Shen, H., Tao, S., and Ma, J.: Modeling the atmospheric transport and outflow  
1244 of polycyclic aromatic hydrocarbons emitted from China, Atmos. Environ., 45, 2820-  
1245 2827, 2011.

1246  
1247 Zhang, Y., Tao, S., Ma, J., and Simonich, S.: Transpacific transport of benzo[a]pyrene  
1248 emitted from Asia: importance of warm conveyor belt and interannual variations, Atmos.  
1249 Chem. Phys, 11, 18879-19009, 2011.

1250  
1251 Zhang, Y., Tao, S., Shen, H., and Ma, J.: Inhalation exposure to ambient polycyclic  
1252 aromatic hydrocarbons and lung cancer risk of Chinese population, PNAS, 106, 21063-  
1253 21067, 2009.

1254

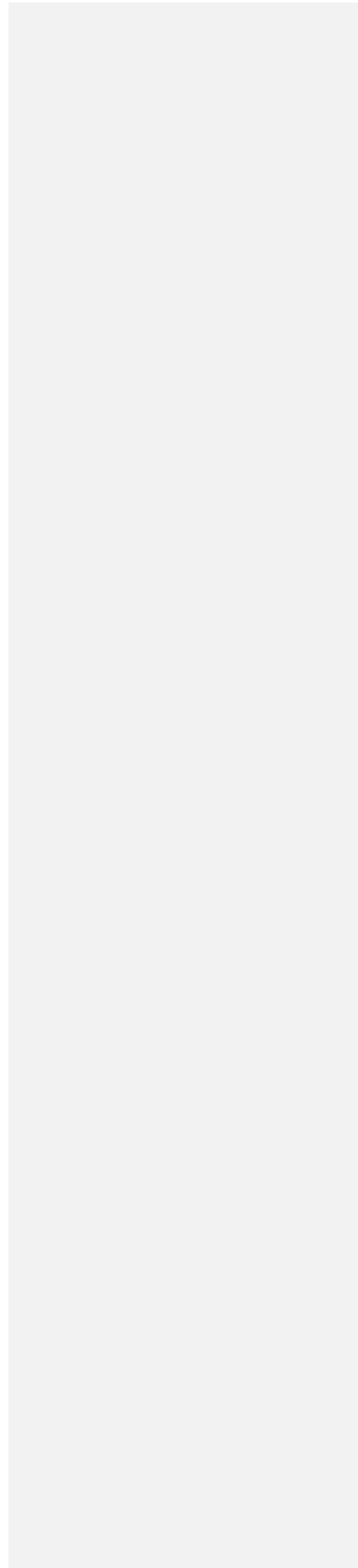
**Formatted:** Font: (Default) Times  
New Roman, 12 pt, Not Bold

**Formatted:** Font: (Default) Times  
New Roman, 12 pt, Not Bold

**Formatted:** Font: (Default) Times  
New Roman, 12 pt, Not Bold

**Formatted:** Font: (Default) Times  
New Roman, 12 pt, Not Bold

1255  
1256  
1257





1258 **List of Figures**

1259

1260 **Figure 1:** Map of modelled (JP) annual average total (gas + particle) fluoranthene  
1261 concentrations ( $\text{ng m}^{-3}$ ).

1262

1263 **Figure 2:** Map of measurement stations used in AURAMS-PAH evaluation.

1264

1265 **Figure 3:** All-site ensemble of modelled-to-measured concentration ratios for total (gas +  
1266 particle) PAHs using JP and DE partitioning expressions.

1267

1268 **Figure 4:** All-site ensemble of modelled-to-measured concentration ratios for total (gas +  
1269 particle) PAHs using JP partitioning expression plotted by month. (a) PHEN, (b) PYR.

1270

1271 **Figure 54:** Site-specific modelled-to-measured concentration ratios for total (gas +  
1272 particle) fluoranthene for JP partitioning.

1273

1274 **Figure 65:** All-site ensemble of modelled-to-measured PAH particulate fraction ratios for  
1275 JP and DE partitioning expressions.

1276

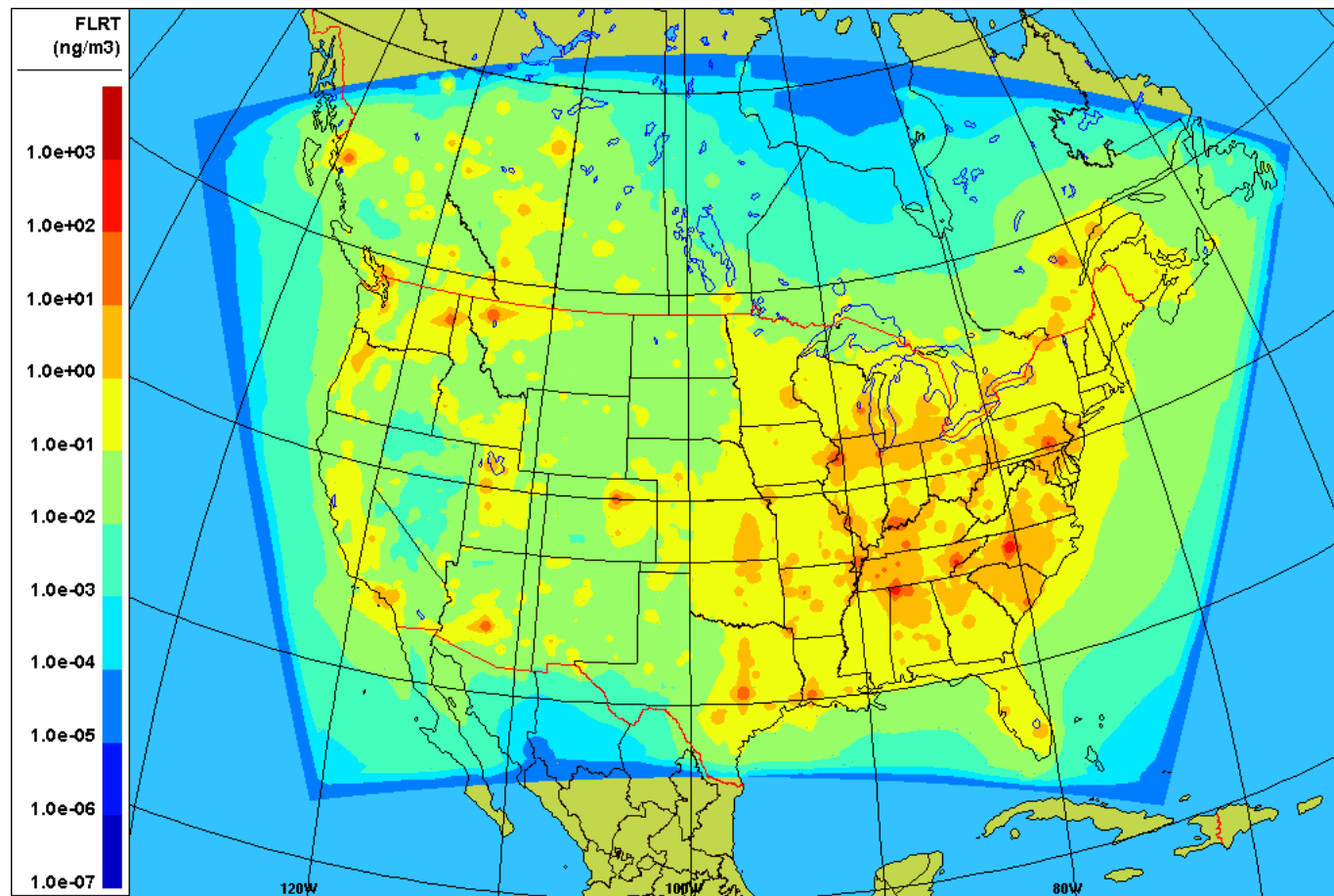
1277 **Figure 76:** Site-specific modelled-to-measured partition coefficients for fluoranthene for  
1278 DE partitioning for eight IADN sites.

1279

Formatted: Font: Not Bold

1280 **Figure 1: Map of modelled (JP) annual average total (gas + particle) fluoranthene concentrations ( $\text{ng m}^{-3}$ ).**

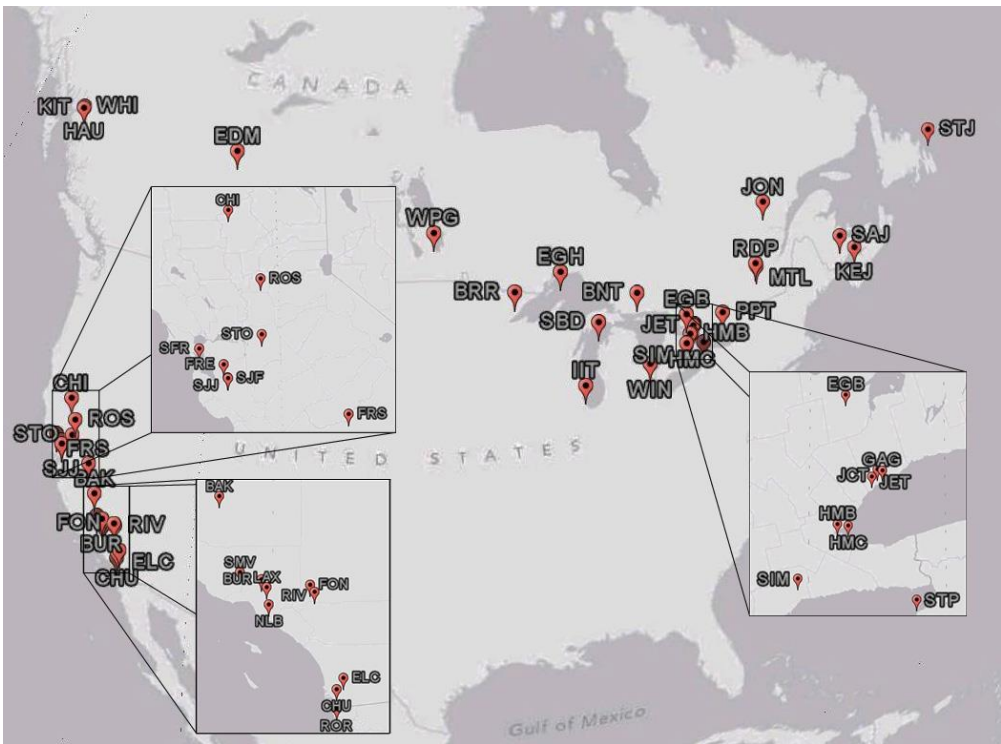
1281



1282

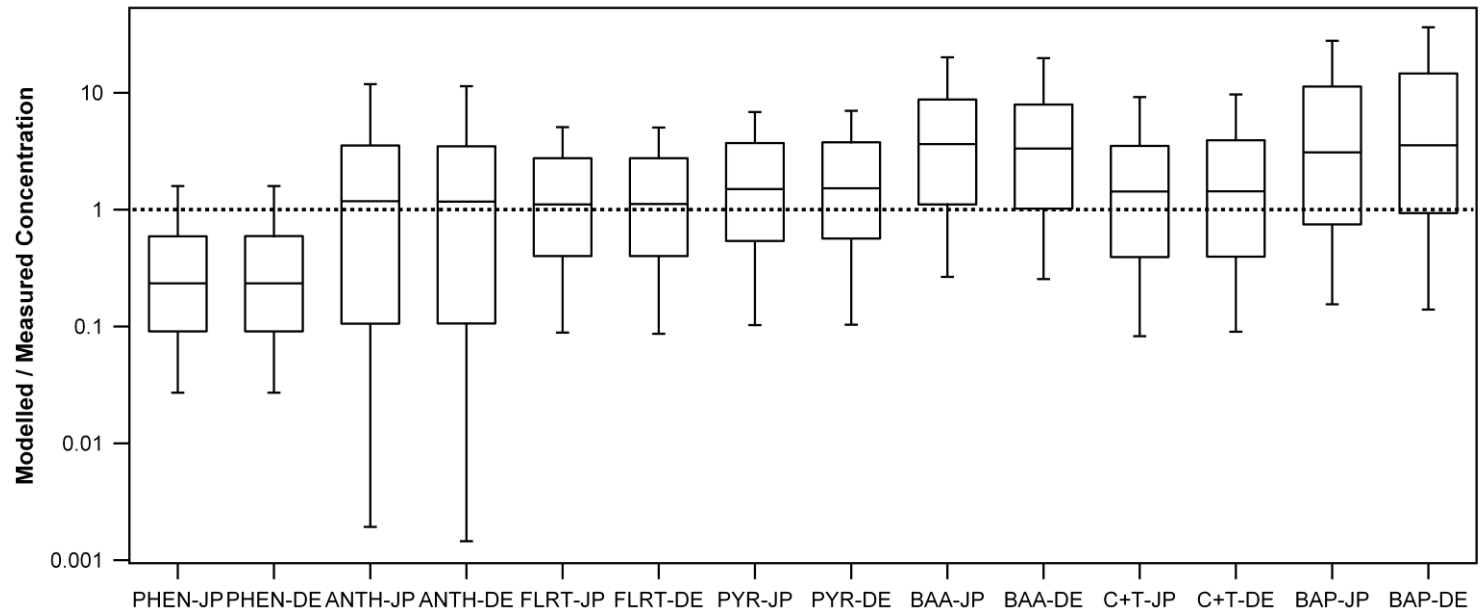
1283  
1284

Figure 2: Map of measurement stations used in AURAMS-PAH evaluation.



1285  
1286

1287 **Figure 3: All-site ensemble of modelled-to-measured concentration ratios for total (gas + particle) PAHs using JP and DE**  
1288 **partitioning expressions.**  
1289



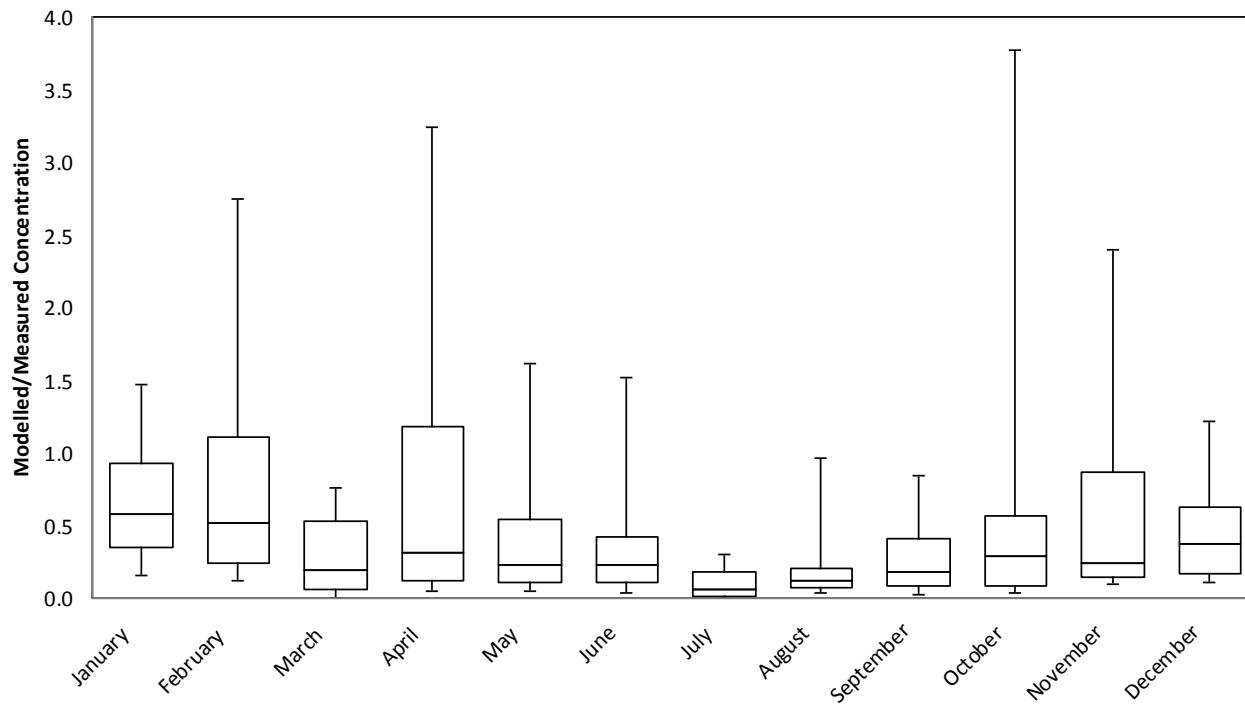
1290 N.B. Box boundaries are 25<sup>th</sup>, 50<sup>th</sup> and 75<sup>th</sup> percentile values; whiskers are 10<sup>th</sup> and 90<sup>th</sup> percentile values. JP = Junge-Pankow partitioning; DE = Dachs-  
1291 Eisenreich partitioning.  
1292

1293  
1294  
1295  
1296  
1297  
1298  
1299

1300  
1301  
1302  
1303

**Figure 4:** All-site ensemble of modelled-to-measured concentration ratios for total (gas + particle) PHEN (a) and PYR (b) using JP partitioning expression plotted by month.

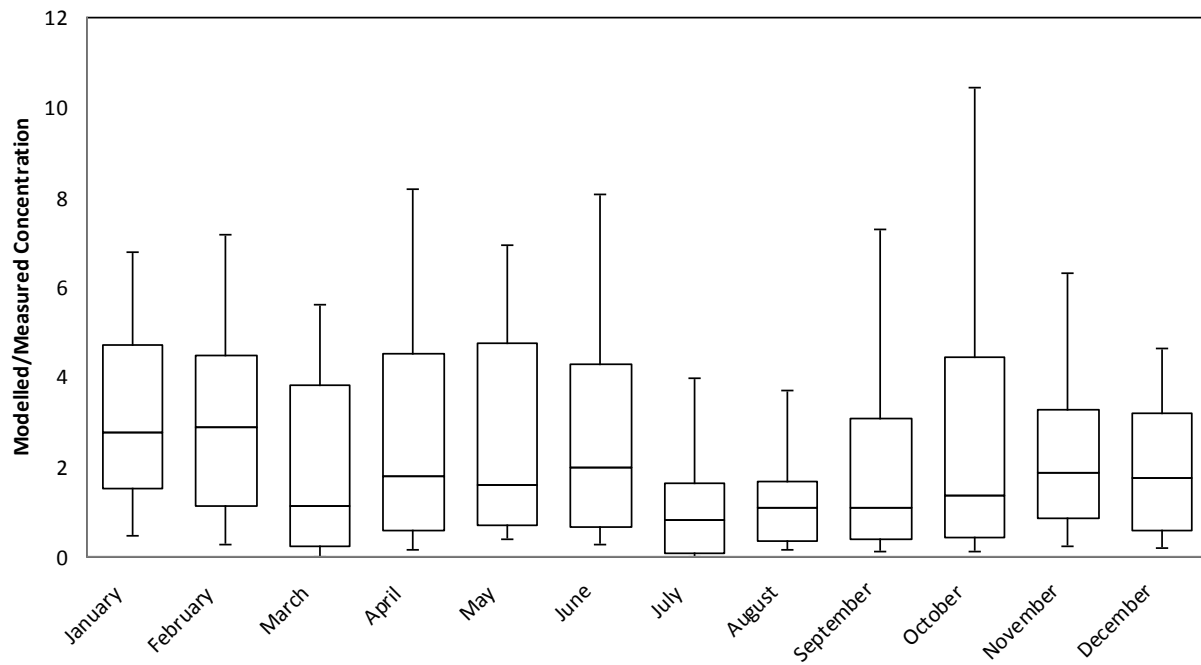
(a) PHEN



1304  
1305  
1306  
1307

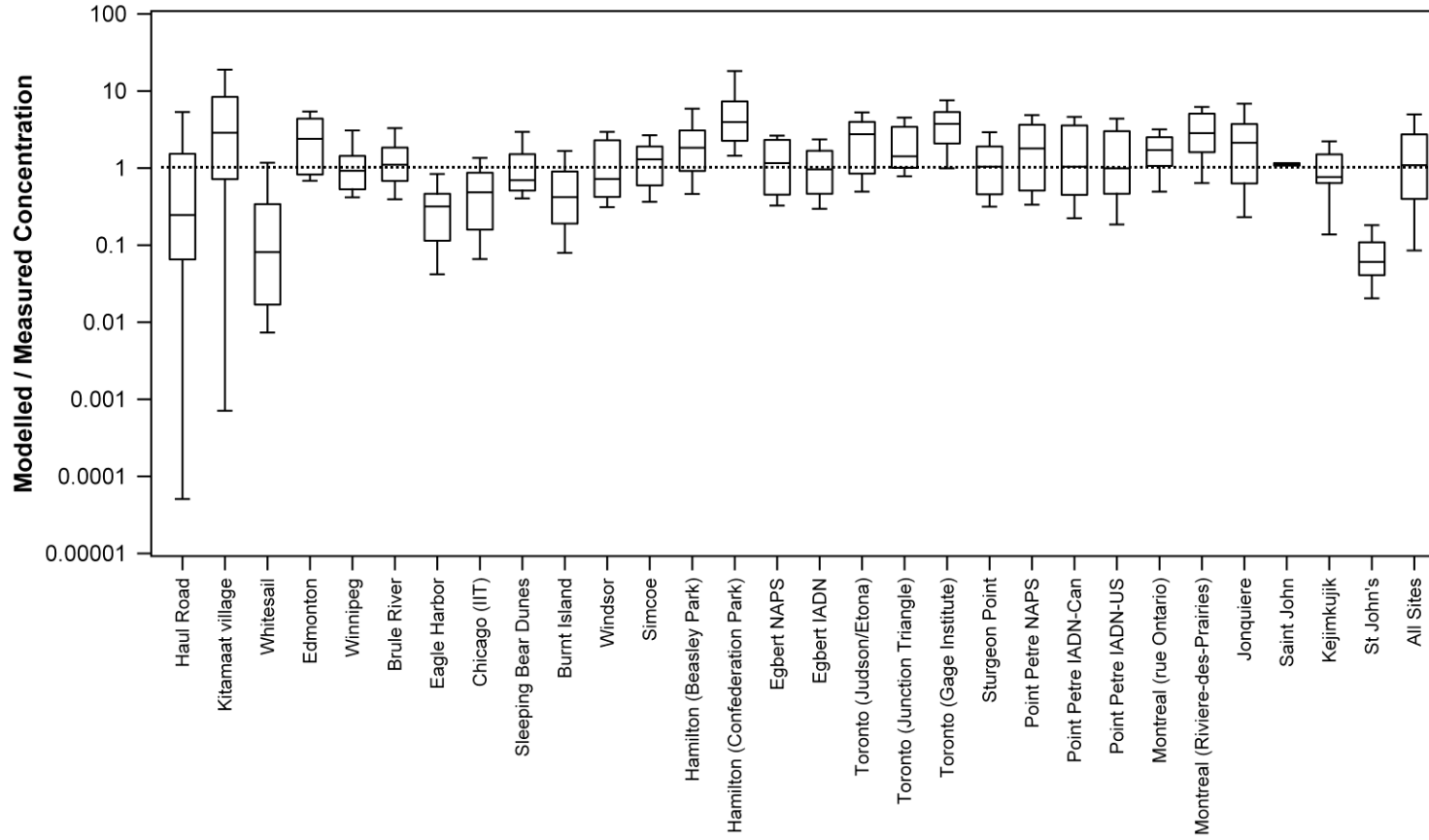
1308

[\(b\) PYR](#)



1309

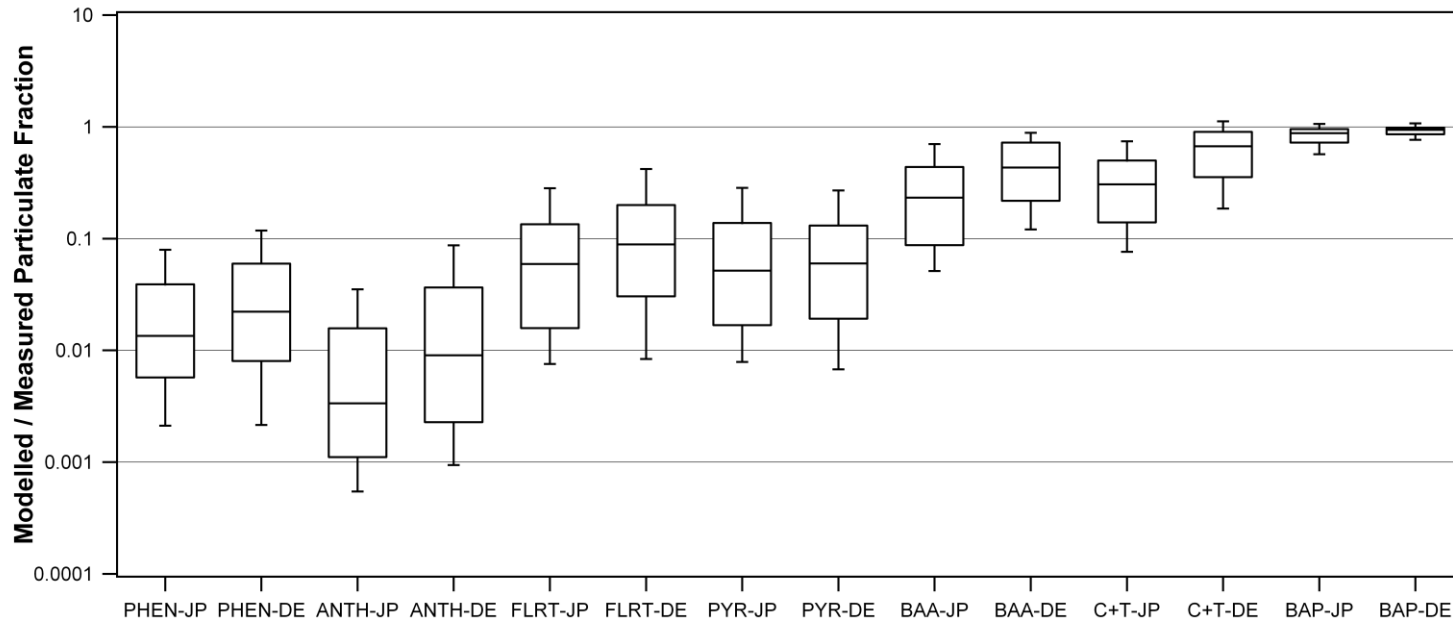
1310 | Figure 45: Site-specific modelled-to-measured concentration ratios for total (gas + particle) fluoranthene for JP partitioning



1311 N.B. Box boundaries are 25<sup>th</sup>, 50<sup>th</sup> and 75<sup>th</sup> percentile values; whiskers are 10<sup>th</sup> and 90<sup>th</sup> percentile values.  
1312

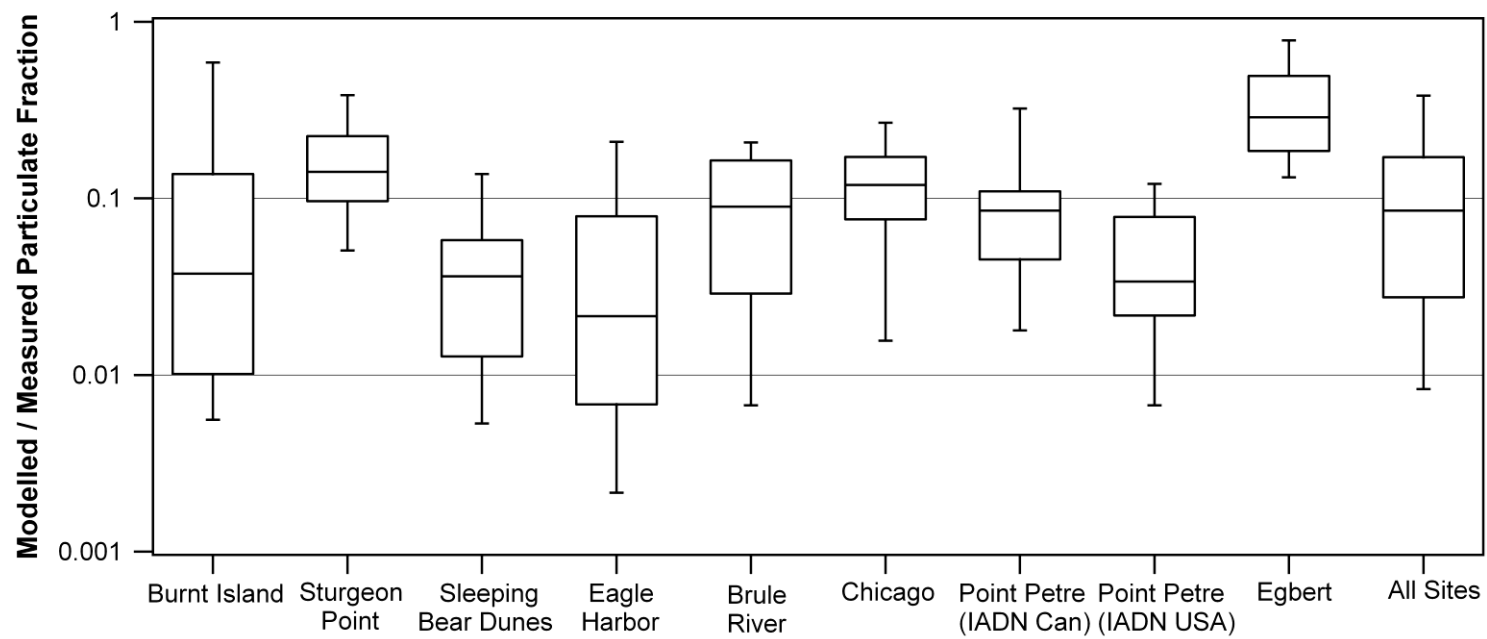


1313 | **Figure 65: All-site ensemble of modelled-to-measured PAH particulate fraction ratios for JP and DE partitioning expressions.**  
1314



1315  
1316  
1317 N.B. Box boundaries are 25<sup>th</sup>, 50<sup>th</sup> and 75<sup>th</sup> percentile values; whiskers are 10<sup>th</sup> and 90<sup>th</sup> percentile values. JP = Junge-Pankow partitioning; DE = Dachs-  
1318 Eisenreich partitioning.  
1319  
1320  
1321  
1322  
1323

1324 | **Figure 76: Site-specific modelled-to-measured partition coefficients for fluoranthene for DE partitioning for eight IADN sites.**  
1325



1326  
1327  
1328 | N.B. Box boundaries are 25<sup>th</sup>, 50<sup>th</sup> and 75<sup>th</sup> percentile values; whiskers are 10<sup>th</sup> and 90<sup>th</sup> percentile values.  
1329  
1330  
1331

